ISTANBUL TECHNICAL UNIVERSITY ★ ENERGY INSTITUTE

CRYSTAL STRUCTURE PREDICTION AND AMMONIA DYNAMICS IN STRONTIUM AMMINE COMPLEX

M.Sc. THESIS

Mehmet ÇANKAYA

Energy Science and Technology Division

Energy Science and Technology Programme

DECEMBER 2016

ISTANBUL TECHNICAL UNIVERSITY ★ ENERGY INSTITUTE

CRYSTAL STRUCTURE PREDICTION AND AMMONIA DYNAMICS IN STRONTIUM AMMINE COMPLEX

M.Sc. THESIS

Mehmet ÇANKAYA
(301131016)

Energy Science and Technology Division

Energy Science and Technology Programme

Thesis Advisor: Assoc. Prof. Adem TEKİN

DECEMBER 2016

İSTANBUL TEKNİK ÜNİVERSİTESİ ★ ENERJİ ENSTİTÜSÜ

STRONSİYUM AMİN KOMPLEKSİNİN KRİSTAL YAPI TAHMİNİ VE AMONYAK DİNAMİĞİNİN ANALİZİ

YÜKSEK LİSANS TEZİ

Mehmet ÇANKAYA
(301131016)

Enerji Bilim ve Teknoloji Anabilim Dalı

Enerji Bilim ve Teknoloji Programı

Tez Danışmanı: Doç. Dr. Adem TEKİN

ARALIK 2016

Mehmet Çankaya, a M.Sc student of ITU Energy Instıtute 301131016, successfully defended the thesis “CRYSTAL STRUCTURE PREDICTION AND AMMONIA DYNAMICS IN STRONTIUM AMMINE COMPLEX, which he prepared after fulfilling the requirements specified in the associated legislations, before the jury whose signatures are below.

Thesis Advisor : **Assoc. Prof. Dr. Adem TEKİN** ....
Istanbul Technical University

Jury Members: : **Prof.Dr. Nilgün KARATEPE YAVUZ** ....
Istanbul Technical University

Assoc. Prof. Dr. Şaron ÇATAK ....
Boğaziçi University

Date of Submission : 25 November 2016
Date of Defense : 21 December 2016

To my lovely spouse; Ayşegül,

FOREWORD

I would like to express my sincerest thanks to my advisor Assoc. Prof. Adem TEKİN for his invaluable suggestions, supervision, encouragements during this study.

I would also like to thank my friend Samet for his help and support during the writing period.

Finally, i would like to extend my heartfelt thank to my family for their love and support.

November 2016 Mehmet ÇANKAYA
(Physics Engineer)

TABLE OF CONTENTS

Page

FOREWORD .... **ix**
TABLE OF CONTENTS .... **xi**
ABBREVIATIONS .... **xiiii**
LIST OF TABLES .... **xv**
LIST OF FIGURES .... **xvii**
SUMMARY .... **xix**
ÖZET .... **xxi**
1. INTRODUCTION – **1**
  1.1 Purpose of Thesis 3
  1.2 Literature Review 3
  1.3 The Outline of The Study 5
2. CRYSTAL STRUCTURE PREDICTION **7**
  2.1 CALYPSO 7
  2.2 USPEX 8
  2.3 XtalOpt 8
  2.4 GASP 9
  2.5 EVO 9
  2.6 CASPESA 9
3. METHODOLOGY **13**
  3.1 Schrödinger Equation 13
  3.2 Density Functional Theory (DFT) 14
  3.3 Nudged Elastic Band (NEB) 16
4. RESULTS AND DISCUSSIONS **19**
  4.1 Global Crystal Structure Predictions 19
    4.1.1 Crystal structure predictions for $Sr(NH_3)_8Cl_2$ 19
    4.1.2 Crystal structure predictions for $Sr(NH3)_6Cl_2$ 23
    4.1.3 Crystal structure predictions for $Sr(NH_3)_4Cl_2$ 25
    4.1.4 Crystal structure predictions for $Sr(NH_3)_2Cl_2$ 26
    4.1.5 Crystal structure predictions for $Sr(NH_3)Cl_2$ 28
  4.2 Finding Minumum Energy Paths (MEP) 29
    4.2.1 MEP for NH_3 diffusion in $Sr(NH_3)_8Cl_2$ 29
    4.2.2 MEP for NH_3 diffusion in $Sr(NH3)_6Cl_2$ 31
    4.2.3 MEP for NH_3 diffusion in $Sr(NH_3)_2Cl_2$ 32
    4.2.4 MEP for NH_3 diffusion in $Sr(NH_3)Cl_2$ 33
  4.3 Conclusion 33
REFERENCES **37**
CURRICULUM VITAE **41**

ABBREVIATIONS

CASPESA **:** Crystal Structure Prediction via Simulated Annealing
DFT **:** Density Functional Theory
MEP **:** Minumum Energy Path
MOF **:** Metal Organic Framework
NEB **:** Nudged Elastic Band
SA : Simulated Annealing

LIST OF TABLES

Page

Table 4.1 : The energies, crystal symmetries and the cell parameters of the $Sr(NH_3)_8Cl_2$ structures. **24**
Table 4.2 : The energies, crystal symmetries and the cell parameters of the $Sr(NH_3)_6Cl_2$ structures.. **26**
Table 4.3 : The energies, crystal symmetries and the cell parameters of the $Sr(NH_3)_4Cl_2$ structures. **28**
Table 4.4 : The energies, crystal symmetries and the cell parameters of the $Sr(NH_3)_2Cl_2$ structures. **30**
Table 4.5 : The energies, crystal symmetries and the cell parameters of the $Sr(NH_3)Cl_2$ structures. **32**

LIST OF FIGURES

Page

Figure 1.1 : Schematic illusration of reversible process of ammonia ab– and desorption in Mg(NH3)6Cl2 [5] **4**

Figure 2.1 : Capped trigonal prismatic structure of $Sr(NH_3)_7$. Sr: yellow, N: blue, H:white. **10**

Figure 2.2 : The example model structure that was used in CASPESA. Cl atoms are represented with green colour............ **11**

Figure 4.1 : The experimental and its relaxed structures of $Sr(NH_3)_8Cl_2$. a) The experimental structure at 293K [50]. b) The DFT optimized experimental structure. **17**

Figure 4.2 : The bond distances between Sr – N atoms of $Sr(NH_3)_8Cl_2$. a) The experimental structure at 293 K [9]. b) The DFT optimized experimental structure.. .... **18**

Figure 4.3 : The bond distances between Sr – N atoms of $Sr(NH_3)_8Cl_2$. a) The experimental structure at 275 K [10]. b) The DFT optimized experimental structure.. .... **19**

Figure 4.4 : The bond distances between Sr – N atoms of $Sr(NH_3)_8Cl_2$. a) The experimental structure at 322 K [10]. b) The DFT optimized experimental structure.. .... **19**

Figure 4.5 : Six different coordination for the structure prediction of $Sr(NH_3)_8Cl_2$. **20**

Figure 4.6 : $Sr(NH_3)_8Cl_2$ structures with the lowest energies **21**

Figure 4.7 : The chlorine – hydrogen distances in N8_1 structure. **22**

Figure 4.8 : Two different coordination for the structure prediction of $Sr(NH_3)_6Cl_2$**23**

Figure 4.9 : $Sr(NH_3)_6Cl_2$ structures with the lowest energies. **23**

Figure 4.10 : The chlorine – hydrogen distances in N6_1 structure. **24**

Figure 4.11 : Two different coordination for the structure prediction of $Sr(NH_3)_4Cl_2$ **24**

Figure 4.12 : $Sr(NH_3)_4Cl_2$ structures with the lowest energies. **25**

Figure 4.13 : The chlorine – hydrogen distances in N4_1 structure. **26**

Figure 4.14 : The model used for the crystal structure prediction of $Sr(NH_3)_2Cl_2$. **26**

Figure 4.15 : $Sr(NH_3)_2Cl_2$ structures with the lowest energies **27**

Figure 4.16 : The chlorine – hydrogen distances in N2_1 structure. **28**

Figure 4.17 : The model used for the crystal structure prediction of $Sr(NH_3)Cl_2$. . **28**

Figure 4.18 : $Sr(NH_3)Cl_2$ structures with the lowest energies **29**

Figure 4.19 : Minumum energy path for free NH3 diffusion in $Sr(NH_3)_8Cl_2$ (" i " refers to initial, " s " refers to saddle, and " f " refers to final point) **30**

Figure 4.20 : Minumum energy path for free NH3 diffusion in $Sr(NH_3)_8Cl_2$ (free NH_3 moves to vacant position on Sr atom)............ **31**

Figure 4.21 : Minumum energy path for bounded NH3 diffusion in $Sr(NH_3)_8Cl_2$... **31**

Figure 4.22 : Minumum energy path for NH3 diffusion in $Sr(NH_3)_6Cl_2$............ **32**

Figure 4.23 : Minumum energy path for NH3 diffusion in $Sr(NH_3)_2Cl_2$............ **33**

Figure 4.24 : Minumum energy path for NH3 diffusion in $Sr(NH_3)Cl_2$............ **34**

Figure 4.25 : Calculated desorption enthalpies (yellow line) versus experimental desorption enthalpies (blue line) for desorption steps of 8 -> 1 and 1 -> 0 of strontium ammine. The lowest energy barriers calculated for NH3 diffusion are represented in red squares. **34**
Figure 4.26 : Calculated desorption enthalpies (yellow line) versus experimental desorption enthalpies (blue line) for desorption steps of 8 -> 2 and 2 -> 1 of strontium ammine. The lowest energy barriers calculated for NH3 diffusion are represented in red squares. **35**

CRYSTAL STRUCTURE PREDICTION OF STRONTIUM AMMINE COMPLEX & ANALYSIS OF AMMONIA DYNAMICS

SUMMARY

In parallel with the rapid technological and economic developments around the world the life standarts get higher and the world population increases and various structural changes that come with them are rapidly increasing the world energy requirement. On the other hand, the reserves of fossil fuels that are presented to us by nature and which are a source of energy that we have been using exessively in the last century are in rapid depletion. Besides the limited amount of these reserves, fossil fuels produce the greenhouse gases as a result of burning the fuel which causes very serious problems for our world. Because of these reasons, it is obvious that alternative energy sources are needed to be developed irrespective of how much fossil fuel reserves remain.

Hydrogen which is the most abundant element in the planet is a promising alternative energy source that it has significant properties and a great potential as an energy carrier. It has high energy density and is a relatively clean energy source compared to fossil fuels. However, there are some difficulties in using hydrogen as an energy source; the hydrogen production and storage at high efficiency are big challenges.

The main goal when storing hydrogen is to achieve the highest possible volumetric density in storage. The second important criterion is the reversibility of hydrogen in absorption and desorption. In order to provide all these desired properties in the best way, many studies have been conducted on storage techniques of hydrogen. These storage techniques can be examined in three main categories as gas, liquid, solid phase.

Gas phase storage is generally carried out in high pressure vessels with a pressure of 20 MPa. Depending on the weight and type of the tank, 1 – 7 wt % hydrogen can be stored. The new generation of lightweight composite cylinders can withstand pressures up to 80 MPa and at this pressure hydrogen can be stored up to a volume of 36 kg-m^3. It is an economical solution compared to other methods, but due to the fact that the energy density of hydrogen is very low, the amount of stored hydrogen in mass is limited. Furthermore, about 20 % of the fuel energy is spent to compress the hydrogen during storage.

Liquid storage is made in super insulated double-walled cryogenic vessels that minimize heat transfer and boiling. In comparison to gas storage it is relatively light method, but since cryogenic temperature is required for this storage to be made, the energy required for liquefaction is very high.

Solid storage can be done with the help of metal hydrides, carbon nanotubes, metal organic frameworks (MOF) and metal amines. In storage with metal hydrides, hydrogen is chemically in interaction with metal atoms and upon the thermal treatment hydrogen releases. Storage with metal hydrides; reliable, requires little space and less energy to refill compare to gas and liquid storage. Despite these advantages, this method also has some disadvantages such as high energy requirement, heavy weight and high cost in releasing the fuel. All reversible hydrides operating at normal

temperature and atmospheric pressure contain transition metals, so that the gravimetric storage capacity of hydrogen is less than 3 %. Carbon nanotubes are tubular transformed graphite sheets with dimensions in microns. Nanotubes can be produced in single-wall or multi-wall forms, and there are also nanotubes formed with various additives such as alkali metals (Li, K). Hydrogen storage capacities of carbon nanotubes vary according to the type of nanotube (single-walled, multi-walled), whether tubes are close or open, the measurements of the tube (tube diameter, length etc.) and the activity of the tube surfaces. Some of the carbon nanotubes obtained in the studies have shown to have a very high hydrogen capacity. However, very low temperatures and high pressures are required to achieve this high capacity. Moreover, the cost of nanotubes is high and the technologies and facilities available today are not sufficient to produce high amounts of carbon nanotubes. Metal organic frameworks (MOFs, Metal Organic Frameworks) are chemical compounds with high porosity, containing a metal ion or ions that coordinated with an organic molecule. This porous system provides a high surface area for hydrogen absorption. Although 4.5 wt % hydrogen can be stored at cryogenic temperatures, the hydrogen storage capacity at room temperature is about 1 wt %. Metal amine compounds have an easier absorption and release kinetics than metal hydrides. Although metal amines are known compounds for about a century, hydrogen storage with these structures is a new concept. Their general formula is $M(NH_3)_nX_m$ where M is a metal cation (Sr, Mg, Ca, Cr, Zn ...), and X is an anion such as Cl, SO_4. Molecular ammonia contains 17.8 wt % of hydrogen and it can be used as a direct fuel in internal combustion engines or in solid oxide fuel cells or it can be catalyzed to hydrogen and nitrogen molecules below 650 K with high efficiency. Although pure ammonia carries a high amount of hydrogen, it is not safe to use it alone due to its toxicity. Therefore, storing ammonia in the form of metal ammines also solves the transportation of ammonia. The great advantage of this method is that the absorption and release of ammonia are reversible, fast and easy to control.

In this study, metal amine compounds of $Sr(NH_3)_nCl_2$ (for n=8, 6, 4, 2, 1) were investigated. Strontium metal ammine complex carry great potential as an energy carrier. In the literature, it has been stated that this compound can store hydrogen up to 8.21 wt % at a temperature of 273 K and pressure of 1 bar so that the ammonia release can start at suitable temperatures which are not so high for practical use. Moreover, $SrCl_2$ can absorb eight ammonia molecules per unit formula, which theoretically corresponds to a volumetric density of 642 kg - $(NH3)m^{-3}$ at room temperature. Considering this great potential, it was aimed to determine the lowest energy structures of strontium ammine compounds and analyze their ammonia dynamics in the recent study. At first, crystal structure prediction was performed to find the unknown crystal structures using CASPESA method which is a crystal structure prediction program developed by our research group. The resulting structures from CASPESA were further optimized with the DFT. The best DFT structures were applied to phonon calculations to select the stable structures. Then, the selected structures have been employed in the nudged elastic band calculations to reveal the ammonia dynamics.

STRONSİYUM AMİN KOMPLEKSİNİN KRİSTAL YAPI TAHMİNİ VE AMONYAK DİNAMİĞİNİN ANALİZİ

ÖZET

Dünya genelinde artan teknolojik ve ekonomik gelişmelere paralel olarak hayat standartlarının yükselmesi, dünya popülasyonunun artması ve bunlarla birlikte gelen çeşitli yapısal değişiklikler, dünya enerji gereksinimi hızlıca artırmaktadır. Buna karşılık doğa tarafından bize sunulan ve sanayi devrimi ile birlikte son yüzyılda oldukça fazla kullandığımız enerji kaynağı olan fosil yakıtların rezervleri ise gün geçtikçe azalmaktadır. Bu rezervlerin sınırlı miktarda olmasının dışında, fosil yakıtların çok fazla tüketilmesi ve bu tüketimin çok hızlı bir biçimde artması, yanma sonucu açığa çıkan sera gazlarını da artırmaktadır ve bu durum dünyamız için çok ciddi sorunların oluşmasına neden olmaktadır. Bu nedenlerden dolayı, ne kadar fosil yakıt kaldığına bakmaksızın alternatif enerji kaynaklarının geliştirilmesi gerekliliği açıkça görülmektedir.

Evrende en çok bulunan hidrojen, önemli özelliklere sahip olduğundan ve enerji taşıyıcı olarak büyük bir potansiyele sahip olmasından dolayı umut veren alternatif enerji kaynaklarındandır. Hafiftir, kütlece yüksek enerji yoğunluğuna sahiptir ve kimyasal enerjiyi direkt olarak elektrik enerjisine çeviren yakıt hücreleri için oldukça efektiftir. Bu özelliklerinin yanı sıra, fosil yakıtlara kıyasla oldukça temiz bir enerji kaynağıdır. Fakat, hidrojenin enerji kaynağı olarak kullanılmasında bazı zorluklar vardır. Hidrojen sadece enerji taşıyıcısı olarak kullanılır, direkt enerji kaynağı değildir. İhtiyaç duyulan yerde ve zamanda hidrojen kullanılabilmesi için, üretilirken depolanması gerekir. Ancak hidrojenin üretimi ve yüksek verimle depolanması kolay değildir. Doğada bulunan en hafif element olduğundan, depolamada büyük hacimler gerekir. Normal şartlar altında, atmosfer basıncında, 1 kg hidrojen gazı 11 m^3 yer kaplar.

Hidrojen depolarken ana amaç, depolamada mümkün olan en yüksek hacimsel yoğunluğa ulaşmaktır. İkinci önemli kriter ise hidrojenin salınımı ve geri alınımının tersinir olmasıdır. Bu kriterleri sağlarken, depolamadaki maliyeti, mümkün olduğunca en uygun seviyede tutmak gerekir. Tüm bu istenilen özellikleri en iyi şekilde sağlayabilmek için hidrojen depolama teknikleri üzerine birçok çalışma yapılmıştır ve yapılmaya da devam edilmektedir. Bu depolama teknikleri, gaz, sıvı ve katı fazda olmak üzere üç ana kategoride incelenebilir.

Gaz fazda depolama, genel olarak maximum basıncı 20MPa olan yüksek basınçlı kaplarda yapılır. Tankın ağırlığına ve tipine göre ağırlıkça % 7 hidrojen depolanabilmektedir. Yeni nesil hafif kompozit silindirler 80MPa'ya kadar basınca dayanabilir ve bu basınçta hidrojen hacimsel olarak 36 $kg\text{-}m^{-3}$ miktarına kadar depolanabilir. Diğer yöntemlere göre ekonomik bir depolama yöntemidir, fakat hidrojenin enerji yoğunluğunun oldukça düşük olması, depolanan kütlece hidrojen miktarının yetersiz kalmasına neden olabilmektedir. Üstelik kullanılan basınçlı kapların yeterince güvenli olması gerekir ve bu nedenle hidrojen depolayan kapların boş ağırlığı da fazla olmaktadır. Bu sebeple hidrojeni gaz halde depolama pratik

kullanım için pek uygun değildir, fakat sabit depolamalar için kullanılabilir. Ayrıca, depolama sırasında hidrojenin sıkıştırılabilmesi için, hidrojen gazının yakıt enerji değerinin yaklaşık % 20 kadarı harcanmaktadır.

Sıvı halde depolama ise, ısı transferini ve kaynama olayını minimize eden süper yalıtımlı olarak dizayn edilmiş çift cidarlı kriyojenik kaplarda yapılır. Gaz halde depolamaya göre nispeten hafif bir depolamadır, fakat bu depolamanın yapılabilmesi için kriyojenik sıcaklık gerektiğinden sıvılaştırma için gerekli enerji büyüktür. Özellikle büyük miktarlardaki depolamalar için maliyeti oldukça yüksektir. Hidrojen enerjisinin yaklaşık % 40'ı sıvılaştırma işlemi için kullanılır. Bunun dışında, hidrojenin sahip olduğu düşük kritik sıcaklık (33 K) yüzünden çok iyi yalıtılmış kapta oluşan ısı transferi, kap basıncının yükselmesine neden olur ve basıncı dengelemek için buharlaşan hidrojenin atmosfere atılması gerekir. Bu durum, depolama ve kullanım sırasında buharlaşma kayıpları meydana getirir.

Gaz ve sıvı haldeki depolamaların bu zayıf yönlerine kıyasla, katı fazda depolamanın avantajları daha fazladır. Katı depolama ise metal hidrürler, karbon nanotüpler, metal organik kafes yapılar ve metal aminler yardımı ile yapılabilir. Metal hidrürler ile depolamada, hidrojen, metallerin atomları arasındaki boşlukta depolanır ve kullanım sırasında hidrojen salınımı termal olarak sağlanır. Metal hidrürler ile depolama; güvenilirdir, az yer kaplar, gaz ve sıvı depolamanın aksine yeniden doldurulmada az enerji gerektirir. Bu gibi avantajlara sahip olmasına rağmen, yakıtın dışarıya salınımı sırasında yüksek enerji gereksinimi, ağır ve pahalı olması gibi dezavantajları vardır. Normal sıcaklık ve atmosfer basıncı seviyesinde çalışan tüm tersinir hidürler geçiş metalleri içerir, bu nedenle kütlece hidrojen depolama kapasitesi % 3'den azdır. Karbon nanotüpler, grafit levhaların tüp hale dönüştürülmüş halidir, boyutları mikron seviyesindedir. Nanotüpler tek duvarlı veya çok duvarlı şekilde üretilebilmektedir, ayrıca alkali metal ilaveli (Li, K) vb. gibi çeşitli ilavelerle oluşturulan nanotüpler de bulunmaktadır. Karbon nanotüplerin hidrojen depolama kapasiteleri nanotüpün farklı özelliklerine göre farklılıklar göstermektedir. Bunlar sırasıyla nanotüpün cinsi (tek duvarlı, çok duvarlı), tüplerin kapalı veya açık olması, tüp ölçüleri (tüp çapı, uzunluğu vb.) ve tüp yüzeylerinin aktifliği gibi özelliklerdir. Yapılan çalışmalarda elde edilen bazı karbon nanotüplerin oldukça yüksek hidrojen kapasitesine sahip olduğu görülse de, bu yüksek kapasiteye ulaşabilmek için çok düşük sıcaklıklar ve yüksek basınç gerektiği gözlenmiştir. Ayrıca, karbon nanotüplerin maliyetinin yüksek olması ve yüksek miktarda karbon nanoyapıların üretilmesi için günümüzde kullanılan teknoloji ve imkanların yeterli olmaması, karbon nanotüplerin diğer dezavantajlarıdır. Metal organik kafes yapılar (MOFs, Metal Organic Frameworks), yüksek gözenekliliğe sahip, bir metal iyonu veya bir organik molekül ile koordine edilmiş iyonlar içeren kimyasal bileşiklerdir. Bu gözenekli sistem, hidrojen emilimi için yüksek bir yüzey alanı sağlar. Kriyojenik sıcaklıklarda ağırlıkça % 4.5 hidrojen depolanabilmesine rağmen, oda sıcaklığında hidrojen depolama kapasitesi ağırlıkça % 1 civarındadır. Metal amin bileşikler, metal hidrürlere kıyasla daha kolay emilim ve geri salınım kinetiğine sahiptirler. Metal aminler, yaklaşık yüzyıldır bilinen bileşikler olmasına ragmen, bu yapılar ile hidrojen depolama yeni sayılabilecek bir yöntemdir. Genel formülü $M(NH_3)_nX_m$ olmak üzere, M bir metal katyon (Sr, Mg, Ca, Cr, Zn…), X ise Cl, SO_4 gibi bir anyondur. Bu teknikte hidrojen depolayarak enerji taşıma amonyak yardımı ile olur. Moleküler amonyak kütlece % 17.8 hidrojen içerir ve direkt yakıt olarak içten yanmalı motorlarda veya katı oksit yakıt hücrelerinde kullanılabileceği gibi, 650 K altında yükek verim ile hidrojen ve azot moleküllerine ayrıştırılarak kullanılabilir. Prensip olarak, saf amonyak tek başına kütlece yüksek miktarda hidrojen depolama özelliği taşımasına rağmen, toksik bir materyal olmasından dolayı direkt bir enerji kaynağı olarak kullanılması güvenli değildir. Bu nedenle metal aminler kullanılarak, amonyak daha stabil ve kontrol edilmesi kolay hale getirilebilmektedir. $M(NH_3)_nX_m$ olarak güvenli bir şekilde tutulup, transfer edilebilen amonyak ihtiyaç duyulduğu zaman bileşikten ayrıştırılıp, katı oksit yakıt hücresine direkt amonyak olarak verilebilir veya azot ve hidrojen moleküllerine ayrılarak, elde edilen hidrojen, yakıt olarak uygun bir yakıt hücresinde kullanılabilir. Amonyağın bileşikten ayrılması termal olarak sağlanır ve gerekli olan sıcaklık bileşiğin kompozisyonuna göre farklılıklar gösterir. Bu yöntemin en büyük avantajı, hidrojeni depolayan amonyağın emiliminin ve geri salınımın tersinir, hızlı ve kontrol edilmesinin kolay olmasıdır.

Bu araştırmada, hidrojen depolayıcı olarak $Sr(NH_3)_nCl_2$ (n=8,7,6,5,4,3,2,1 için) metal amin bileşikleri incelendi. Metal katyon olarak stronsiyum (Sr) ve anyon olarak klorür (Cl_2) seçilmesinin nedeni, stronsiyum klorür metal amin bileşiğinin hidrojen depolayıcısı olarak yüksek bir potansiyel taşımasıdır; literatürde bu bileşiğin 0°C sıcaklık ve 1 bar basınçta, kütlece % 8.21'e kadar hidrojen depolayabileceği ve amonyak salınımının pratik kullanım için çok yüksek olmayan uygun sıcaklıklarda başlayabildiği belirtilmiştir. Bunun yanı sıra, $SrCl_2$, birim formül başına sekiz amonyak molekülü absorbe edebilir ve bu miktar teorik olarak, oda sıcaklığında 642 kg-$(NH_3)\cdot m^{-3}$'lük bir hacimsel yoğunluğa tekabül etmektedir. Bu çalışmada, strontium metal amin bileşiklerinin taşıdığı bu potansiyellerden yola çıkılarak, en düşük enerjiye sahip stabil bileşikler belirlenmeye çalışılmıştır. Bu amaçla çalışmanın ilk aşamasında, benzetilmiş tavlama (simulated annealing) algoritmasına bağlı olarak grubumuz tarafından geliştirilen bir kristal yapı tahmin programı CASPESA (Crystal Prediction via Simulated Annealing) kullanılarak bu bileşikler için bir tarama yapılmıştır ve birçok stronsiyum metal amin bileşiğinin kristal yapısı tahmin edilmiştir. Umut veren yapılar için yoğunluk fonksiyonel teori (YFT) kullanılarak bu bileşiklerin atomik koordinatları ve ağ örgü parametreleri eniyilenmiştir. Bir sonraki aşamada, eniyilenmiş olan bu yapıların stabil olup olmadığının anlaşılabilmesi için fonon (phonon) hesaplamaları yapılmıştır. Stabil olduğu gözlenen bileşiklerin amonyak dinamiğinin analizi yapılmak üzere Dürtülü Elastik Bant (DEB) hesaplamaları yapılmıştır. DEB hesabı sayesinde metal aminden ayrılan amonyağın, bileşikten ayrılırken izlediği yol boyunca gereken enerji miktarı hesaplanarak, mümkün olan en düşük enerjili yol bulunmaya çalışılmıştır.

1. INTRODUCTION

Because of the tecnhological and economical devolopments and the increasing population of the earth, the world energy demand grows rapidly. On the other hand, fossil fuels which are the world's primary energy source have limited reserves and they are facing a rapid depletion. Moreover, the consumption of fossil fuels cause serious problems for the global enviroment. Therefore, new alternative energy sources are needed to be searched to replace fossil fuels. Although there are many energy sources, in most cases they can not be used directly. Thus, they should be converted into fuels and an energy carrier is needed after this convertion. At this point, hydrogen is a great canditate as it is light, enviroment friendly, versatile and efficient energy carrier. However, using hydrogen brings some major challenges for storing it in a safe, compact and efficient way.

There are several hydrogen storage methods in order to overcome these challanges. These methods can be categorized as gas, liquid and solid phase. Hydrogen can be stored as gas in high pressure tanks that are generally operated at maximum pressure of 20MPa but new lightweight composite tanks can be operated up to 80Mpa [1]. Depends on tank's type and weight, they can have 1 – 7 wt % hydrogen capacity. Hydrogen storage in gaseous phase is a cheap method, but it has major problems. Safety storage is the biggest concern to store hydrogen as a gas in high pressures. Liquid hydrogen storage is operated at super isolated cryogenic tanks which minimize the heat transfer. These tanks have higher volumetric hydrogen capacity than high pressure tanks, but large amount of energy is needed to liquefy the hydrogen. Approximately 40 % of hydrogen energy is used for liquefaction [2]. Moreover, due to the low critical temperature (33 K) that hydrogen possesses, the heat transfer of the well-insulated container causes the vessel pressure to rise, thus, the evaporating hydrogen must be thrown into the atmosphere to balance the pressure. This situation leads to hydrogen loss. Solid-state storage of hydrogen has more advantages than gas and liquid hydrogen storage. Storage in solid phase can be managed with various methods like metal hydrides, carbon nanotubes, metal-organic frameworks (MOFs), and metal ammines. Metal hydrides, especially that contains magnesium, lithium, sodium, calcium, boron or aluminum, e.g., MgH_2, $NaAlH_4$, $LiAlH_4$, $LaNi_5H_6$ can be used for hydrogen storage. Metal hydrides have high energy density by volume and they provide high safety but they are heavy and expensive. Moreover, it requires high energy to release hydrogen. Another method in solid phase storage is carbon nanotubes which can be produced as single-walled nanotubes and multi walled nanotubes. Their storage capacity varies according to the nanotube's type (single walled, multi walled), size (diameter,length) and activity of the surface of the nanotube. Although the carbon nanotubes have high potential for hydrogen storage, they have some disadvantages such as they are expensive and high pressure and very low temperature is required for high storage capacity. Metal Organic Frameworks , MOFs, are nanoporous materials that contains metal ions and clusters which are associated with organic units [3]. In 2006, a hydrogen storage value of 7.5 % was reported for MOF-177 material at 77 K [4]. However, the hydrogen capacity of this material is maximum 1 wt % at room temperature and at 20 bar pressure. In comparison to metal hydrides, metal ammine complexes have better hydrogen absorption and release kinetics. Despite metal ammines are known approximately for a century, using them to store hydrogen is a new concept [5]. Their general formula is $M(NH_3)_nX_m$ that M is a metal cation (Sr, Mg, Ca, Cr, Zn …) and X is an anion like Cl, SO_4... Ammonia works as a energy carrier in metal ammines. Molecular ammonia contains 17.8 wt % hydrogen and that can be used directly in solid oxide fuel cells and internal combustine engines or it can be decomposed to hidrogen and nitrogen around 650 K with high efficiency [1]. Theoretically pure ammonia can be used as an energy carrier but that is not safe, because ammonia is a highly toxic material. At this point, metal ammines can be used to make ammonia more stable and easier to handle, e.g for transportation. After storing and transfering ammonia safely by metal ammines, ammonia can be released when it is needed. Ammonia decomposition occur thermally and the required temperature can be various depends on the composition of the complex. The biggest advantage of this method is that adsorption and desorption of ammonia are reversible, fast and easy to control.

1.1 Purpose of Thesis

The analysis of ammonia dynamics in metal ammine complexes take very important role to be able to use these compounds as future energy carrier. Therefore, several metal ammine complexes with several metal cations and anions have been investigated in previous studies to search hydrogen storage capabilities and ammonia dynamics for these systems [5-9]. In this thesis, metal ammine complexes of strontium chlorine salt were investigated. Strontium metal ammine complexes can store up to 8.21% hydrogen by weight at 273 K and 1 bar [6]. In addition, strontium ammine materials have fast and reversible ammonia ab- and desorption kinetics at operating temperature and pressure. In the literature, it has been stated that $Sr(NH_3)_8Cl_2$ releases seven molecules of NH_3 at nearly 308 K °C by forming $Sr(NH_3)Cl_2$ while it releases the last NH_3 molecule around 358 K by forming $SrCl_2$ at a pressure of 1 bar [6]. Considering these important specifications and great potential of strontium ammines, it has been aimed to examine the crystal structures of $Sr(NH_3)nCl_2$ for n = 8, 6, 4, 2, 1 and analyze their ammonia dynamics by investigating the bulk diffusion of NH_3.

1.2 Literature Review

Using metal ammine complexes for storing hydrogen is a relatively new concept. Several metal ammines were studied with different storage capacities and binding energies in the literature. Christensen et al. [5] had investigated $Mg(NH_3)_6Cl_2$. They had observed that can be stored 9.1 wt % hydrogen in the form of ammonia and decomposition of the compound starts around 350K and all hydrogens can be released at temperatures below 620 K with employing an ammonia decomposition catalyst. They stated that this process is totally reversible that hydrogen and nitrogen can form ammonia with a catalyst so that it can be stored as $Mg(NH_3)_6Cl_2$ and when needed ammonia can be released to be used directly in a fuel cell or it can be decomposed into hydrogen and nitrogen again as shown in Figure 1.1. They also compacted saturated $MgCl_2$ salt into a pellet in order to gain high volumetric density. In 2008, Sørensen and co-workers had studied hydrogen storage capacity of $Ca(NH_3)_8Cl_2$, $Mn(NH_3)_6Cl_2$ and $Ni(NH_3)_6Cl_2$ and compared them with $Mg(NH_3)_6Cl_2$ [6]. They reported that $Ca(NH_3)_nCl_2$ has highest storage density to be 9.78 % by weight and that has stable

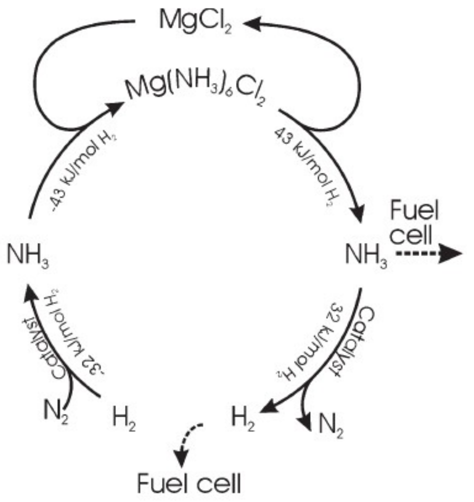

Figure 1.1 : Schematic illusration of reversible process of ammonia ab– and desorption in $Mg(NH_3)_6Cl_2$ [5] .

formation for n = 8, 4, 2, 1 and all of the ammonia desorption occurs between 300 – 550 K. They also observed that $Mg(NH_3)_nCl_2$ storage capacity is 9.19 wt %, $Ni(NH_3)_nCl_2$ capacity is 7.83 wt % and $Mn(NH_3)_nCl_2$ has 7.96 wt % hydrogen storage capacity. $Mg(NH_3)_nCl_2$ is stable for n = 6, 2, 1 and all ammonia desorbtion occur at temperature between 410 - 700 K, $Mn(NH_3)_nCl_2$ have stable structure for n = 6, 2, 1 and all ammonia desorbs in between 350 – 675 K, $Ni(NH_3)_nCl_2$ has stable compositions for n = 6, 2, 1 and all ammonia release in the temperature range of 440 – 700 K. Tekin et al. [7] had investigated ab- and desorption kinectis of ammonia in magnesium ammine from DFT and neutron scattering and they predicted the crystal structures of magnesium hexa-, di- and monoammine by using an algorithm based on simulated annealing (SA). In their study, they predicted a low temperature structure of magnesium hexammine complex in a monoclinic unitcell with space group C2/m (IT: 12). In order to examine ammonia diffusion in $Mg(NH_3)_nCl_2$ with n = 6, 2 ,1, they carried out NEB and ANEB calculations and they calculated the diffusion barriers to be 0.52 – 0.60 eV for hexammine, and they calculated vacancy formation energy to be 0.79 eV along the chain of diammine and 0.66 eV for monoammine interchain pathways. In the another study performed by Churchard et al. [8], crystal structure prediction of $Mg(NH_3)_nCl_2$ with n = 6, 2 ,1 was implemented by a simulated annealing algorithm. They also determined the single and double NH_3 rotations in mangesium hexa-, di- and monoammine complexes and diffusion barriers were calculated for these complexes. The rotational barriers for all NH_3 molecules in $Mg(NH_3)_6Cl_2$ complex were calculated to be 0.09 eV in low temperature phases and three NH_3's rotation barriers were determined to be 0.12, 0.08 and 0.002 eV. Lysgaard et al. [9] had studied the structure of strontium chloride ammines in order to have better understanding of the exact ab- and desorption mechanisms of these complexes. They used DFT calculations and X-ray powder diffraction to determine stable $Sr(NH_3)_nCl_2$ with n = 8, 2, 1 and they confirmed the existence of these phases with space groups of Pnma, Aem2 and Cmcm respectively. They had found the desorption energies of the octa- to diammine , octa- to monoammine and di- to monoammine transitions to be 36.0, 37.9 and 49.4 kJ mol^{-1} respectively at 300 K. In the another recent study performed by Johnsen et al. [10], the crystal structure of strontium chlorine octamine ($Sr(NH_3)_8Cl_2$) had been studied. The structural changes of the complex were investigated for the temperature at 275K and 322K and ammonia pressure at 2.0, 3.4, and 4.4 bar. They reported that the following reactions shown below were observed for the desorbtion of ammonia and the reaction seen in equation 1.1 has the lowest transformation temperature for all pressures that were studied and the reaction seen in equation 1.2 takes important role to lower pressure of ammonia was observed at 2 bar pressure.

$$Sr(NH_3)_8Cl_2 \rightarrow Sr(NH_3)_2Cl_2 + 6NH_3(g) \qquad (1.1)$$

$$Sr(NH_3)_8Cl_2 \rightarrow Sr(NH_3)Cl_2 + 7NH_3(g) \qquad (1.2)$$

They also stated that only one reaction was observed for ammonia absorption as seen in equation 1.3.

$$Sr(NH_3)Cl_2 + 7NH_3(g) \rightarrow Sr(NH_3)_8Cl_2 \qquad (1.3)$$

1.3 The Outline of the Study

Firstly, the crystal structure prediction of strontium metal ammine complex was done via a crystal structure prediction program called CASPESA (CrystAl Structure PrEdiction via Simulated Annealing) which has been developed by our group. Then, $Sr(NH_3)_nCl_2$ structure were predicted for five different NH_3 content (n = 1, 2, 4, 6, 8). For this purpose, model structures were designed for each ammonia content and more than one model were defined for most of the structures. For example, six models were used for the $Sr(NH3)_8Cl_2$. In addition, CASPESA optimization was repeated 500 times for each unit cell type. Considering these huge number of structures, it is not easy to choose the best structures, thus, an analysis script was implemented to evaluate the structures automatically. Then, DFT calculations were performed to relax the best structures by using Dacapo program [11]. The calculations were applicated with a cut off energy of 340 eV for plane wave and 500 eV for the density grid. RPBE [12] exchange – correlation has been used and the ionic cores were defined by ultrasoft pseudopotentials [13]. The electronic Brioullin zones were sampled with (2 x 2 x 2) k-points. After the DFT relaxation, phonon calculations were applied for the best structures. Quantum Espresso [14] was used for these calculations. Finally, the lowest energy barrier and minumum energy paths for bulk diffusion of ammonia were calculated by Nudged Elastic Band (NEB) method [15-19].

2. CRYSTAL STRUCTURE PREDICTION

In order to design new complexes, it is requiered to know the crystal structure of the materials. It is not always possible to find the crystal structure details of desired materials in the literature, at most of the time the knowledge about some materials can be limited. In such cases, crystal structure prediction is essential to provide a crystal structure for desired compounds. For this purpose, many cystal structure prediction techniques have been developed in the literature and in this chapter, the most important ones are going to be mentioned.

2.1 CALYPSO

CALYPSO (Crystal structure AnaLYsis by Particle Swarm Optimization) [20] is an structure prediction method and a computer software which is able to predict the energetically stable or metastable structures at required chemical compositions and external conditions (e.g., pressure, temperature) for 2D layers, 3D crystals, surfaces and clusters. This structure prediction method is based on Particle Swarm Optimization (PSO) which is a stochastic global optimization method that firslty introduced by Kennedy and Eberhart [21,22]. In CALYPSO, global PSO is used for fast convergence and local PSO is used to avoid premature convergence to deal with more compex systems. Moreover, CALYPSO has ben integrated with also some other algorithms and methods such as Artificial Bee Colony algorithm, bond characterization matrix on elimination of similar structures, partial random structures per generation on enhancing structural diversity, symmetry constraints on structural generation, and penalty function, etc.

CALYPSO has been interfaced with VASP, SIESTA, GULP, Quantum Espresso, CP$_2$K, CASTEP code, LAMMPS code, ABACUS code and Gaussian codes. This structure prediction method was implemented to sevaral studies [23-27].

2 USPEX

USPEX (Universal Structure Predictor: Evolutionary Xtallography) has been developed by A. R. Oganov and his co-workers. This method is based on an evolutionary algorithm [28] which is improved by same study group. USPEX also use some alternative methods such as random sampling, corrected particle swarm optimization algorithms, metadynamics. With USPEX, it is possible to obtain structure information by constraining search to fixed experimental cell parameters, of fixed cell shape, or fixed cell volume, searching structures from known or hypothetical structures and gathering crystal structures from predefined molecules, including flexible molecules. USPEX can also be performed for prediction the structure of nanoparticles, polymers, surfaces, interfaces and 2D crystals. It may work efficiently for the systems with up to 100-200 atoms/cell.

USPEX has been interfaced with VASP, QuantumEspresso, GULP, SIESTA, DMACRYS, CP2k, LAMMPS, ATK, MOPAC, FHI-aims, and Gaussian codes. That is also possible to interface with other codes. USPEX method was succesfully used in some studies [29-32].

2.3 XtalOpt

XtalOpt [33-35] is an evolutionary algorithm written in C^{++} to search for the most stable structure in desired composition (the types of unitcell and number of atoms in the unitcell). It is developed from Avogadro [36] molecular editor and it makes use of the OPENBABEL [37,38] chemical toolkit. Some constraints such as a minumum interatomic distance should be set in XtalOpt. Moreover, angles, lattice lenghts and volumes are able to be restrained to a range or be fixed at a single value. In XtalOpt, some mutation operators such as strain, exchange, ripple, crossover operators are defined. Strain operator is used to mutate the unit cell parameters, but not the fractional positions of the atoms. Exchange operator swap two atoms of different types in a cell. Displacement of the atomic coordinates in a cell is performed by the ripple operator. With the crossover operator which is also called as cut and splice operator, two parents are combined to form an offspring.

XtalOpt has been interfaced with VASP, CASTEP, GULP, and Quantum ESPRESSO. This evolutionary algorithm was applied to several studies [39,40].

2.4 GASP

GASP (The Genetic algorithm for structure prediction) is a heuristic search algorithm developed by William W. Tipton, Ben Revard, Stewart Wenner, and Richard G. Hennig [41]. GASP is able to do searches with a variable numbers of atoms in the cell. Moreover, it performs a probability distribution to select structures for mutation, mating and promotion.

It has been interfaced with VASP, LAMMPS, MOPAC, Gulp, and JDFTx. The algorithm can be also run on parallel structures. The GASP program was used in some studies in the literature [42-46].

2.5 EVO

EVO – Evolutionary algorithm for crystal structure prediction has been introduced by Silvia Bahmann and Jens Kortus [47]. Its programming language is Python and operation system is Linux. In EVO, the number of atoms in the conventional cell and multiples of it has been used to find the crystal structures of the elements of the 3rd main group of the periodic system with their different spacegroups. It can also search for 2D structures. It has been interfaced with Quantum ESPRESSO and GULP, and it is also possible to extend it to use other programs in order to calculate total energy of the structures.

2.6 CASPESA

CASPESA is an in-house developed method for crsytal structure prediction and it has been employed in this present study. CASPESA is an efficient program which was succesfully applied before for several complexes like metal ammines [7,8], and metal borohydrides [48-52]. CASPESA uses simulated annealing (SA) algorithm to perform a global optimization. Mostly, SA algorithm is used for minimization, but in this program it is used to maximize the number of formations that can make the crystal structure more stable. Basically, the stabilization of the system is aimed in CASPESA. For this purpose, it is required to know the important components which make the system more stable in order to select initial parameters carefully. Therefore, the bond constraints are taken from the literature if it is possible. Unless there is available data in the literature, CASPESA can be used together with DFT calculations to optimize the structures with incomplete data. In order to understand how this program work, a crystal structure prediction of $Sr(NH_3)_8Cl_2$ material that was studied in this thesis was explained below with details. Firstly, previous studies in the literature were scanned to figure out which factors have effects on stability of the metal ammine complexes. For metal ammine systems, basically two factors may have important role for the stability of the structure; the tendency of alkali earth metals to bond with ammonia and hydrogen bonds between NH_3's hydrogen and chlorine atoms which are implemented as the objective functions in CASPESA. For the structures that were studied in this thesis, interactions between Sr - N and H - Cl bonds were performed as the objective function for the structures that contain a free ammonia molecule (for octammine complexes with seven bounded, a free ammonia molecules), for the other structures only H – Cl bonds were employed as the objective function. The setup of CASPESA is examplified for $Sr(NH_3)_7$ which was modelled as a separate group in the unit cell. Here, Sr is located in the center and six NH_3 have equal distance to Sr (2.83 Å) where one NH_3 is located further (2.89 Å) than other NH_3 groups as they are forming capped trigonal prismatic coordination geometry as seen in Figure 2.1.

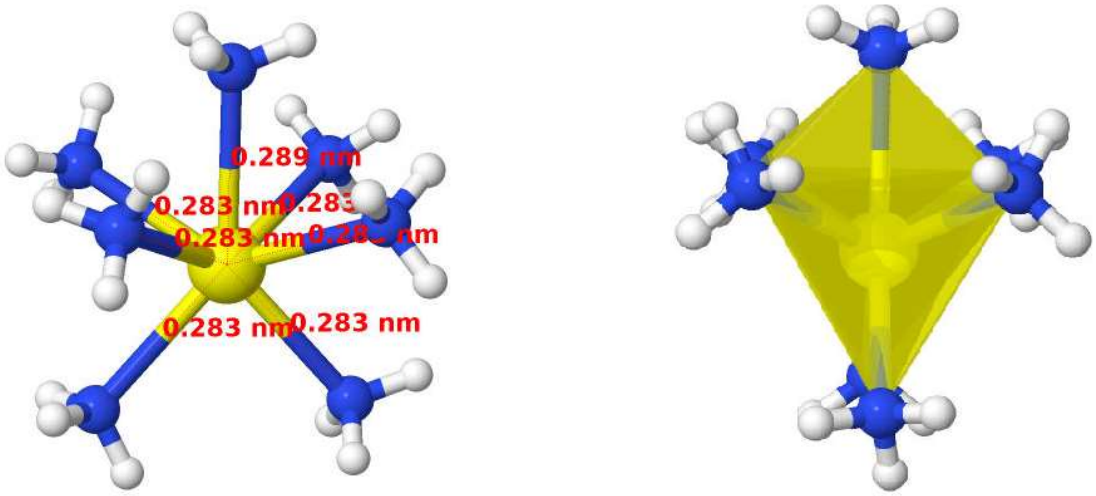

Figure 2.1 : Capped trigonal prismatic structure of $Sr(NH_3)_7$. Sr: yellow, N: blue, H:white

In this example, Sr is at the origin and the choosen example also contains a free NH_3 group and two Cl atoms (Figure 2.2).The chlorine atoms, the $Sr(NH_3)_7$ group and the free NH_3 groups are able to change their positions in the unit cell by using spherical coordinates. Also $Sr(NH_3)_7$ group can rotate around its own center with the help of three euler angles. For all of these movements and rotations 15 parameters are used in this unit cell and extra parameters are added to describe the shape of the unit cell (cubic, tetragonal, monoclinic, orthorhombic, rhombohedral, hexagonal and triclinic). It is required minumum 1 (cubic) and maximum 9 (triclinic) parameters for the description of a unit cell. Thus, the total number of parameters varies in between 16 – 24 to maximize the number of hydrogen bonds in $Sr(NH_3)_8Cl_2$.

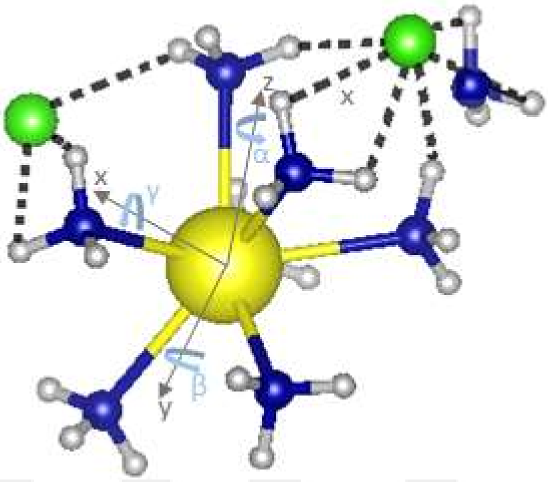

Figure 2.2 : The example model structure that was used in CASPESA. Cl atoms are represented with green colour.

In CASPESA, quantum mechanical or force fields based calculations are not used, and as a consequnce of that, atoms may locate so close to each other that cause non-physical conditions. In order to prevent this situation, bond constraints as mentioned before should be defined in CASPESA. For this structure, minumum interatomic distances were defined according to study of Lysgaard et al. [9]. In particular, the following minimum inter-atomic distances between H-H, Cl-Cl and Cl-Sr atoms were applied respectively as follows 1.65 Å, 5 Å and 3.2 Å.

3. METHODOLOGY

3.1 Schrödinger Equation

As reconsidering de Broglie’s matter wave, Erwin Schrödinger formulated a partial differential equation which was published in 1926. In quantum mechanics, the evolution of an isolated system is given by the time dependent Schrödinger equation that can be seen in equation 3.1:

$$i\hbar \frac{\partial \psi(x,t)}{dx} = \hat{H}\psi(x,t) \tag{3.1}$$

where $\hat{H}$ is the system’s Hamiltonian operator, $\hbar$ is Planck’s constant. The solution of the equation is called as the wave function which comprise all the information about a physical system. The nonrelativistic Hamiltonian for a molecule can be given as a sum of five terms (Equation 3.2):

$$\hat{H} = -\frac{\hbar^2}{2m}\sum_{i} \nabla_i^2 - \sum_{A} \frac{\hbar^2}{2M_A}\nabla_A^2 - \sum_{A,i}\frac{Z_A e^2}{4\pi\epsilon_0 r_{Ai}} + \sum_{i>j}\frac{e^2}{4\pi\epsilon_0 r_{ij}} + \sum_{A>B}\frac{Z_A Z_B e^2}{4\pi\epsilon_0 R_{AB}} \tag{3.2}$$

where i, j refer to electrons and A, B refer to nuclei, M_A denotes the ratio of mass of A to the mass of an electron, R and r denote distances and Z is the nuclear charge. The first two term describes the kinetic energy operator for the electrons and nuclei respectively. The other three terms define the electrostatic interaction between the nuclei and the electrons and repulsive potential due to the electron-electron and nucleus-nucleus interactions respectively. The wave function contains 3N dimensions, where N is the number of electrons. Therefore, when the numbers of electrons increase, explicit solution of the Schrödinger equation becomes exponentially harder. At this point, some accepted approximations like Born-Oppenheimer, Density Functional Theory (DFT), pseudopotential, basis set, supercell approximations etc. can be used to solve the corresponding equations by computers. Among these approximations, Born-Oppenheimer approximation forms the basis for calculation of the most of the electronic structures. It depends on assumption of separating the motion of atomic nuclei and electrons in a molecule. In the first step, the movement of the nuclei is ignored and the Schrödinger equation is solved depending on electrons only, thereby simplifying the equation. In the second step of the approximation, nuclear-nuclear Coulomb term is assumed as a constant and it can be estimated as equation 3.3:

$$E^{nuc} = \sum_{A>B} \frac{Z_A Z_B e^2}{4\pi\epsilon_0 R_{AB}} \qquad 3.3$$

Then, the total energy can be calculated by sum of energy gathered from Schrödinger equation solved based on electrons and the correction from the nuclear energy.

3.2 Density Functional Theory

Density Functional Theory (DFT) is a quantum mechanical theory which is accurate and the most widely used electronic structure method in computational science. This theory simplifies the many-electron Schrödinger equation and with this theory, the electronic structure of many-body systems, particular atoms, molecules, and the condensed phases can be investigated principally at the ground state.

Llewellyn Thomas and Enrico Fermi, in 1927, introduced a model which formed the basis for DFT. By the help of their work, it was realized that if the electron density of a molecule can be determined, numerous things about the molecule could be figured out. Almost 40 years after Thomas-Fermi model, two important theorems which form the fundamental statement of DFT were proved by Hohenberg and Kohn in 1964 [53]. In the first theorem, it was stated that electron density which depends on only x-y-z coordinates of the individual electron determines the ground state properties of a many-electron system. The second theorem characterizes an energy functional for the electronic structure which demonstrates that the precise ground state electron density minimizes this energy functional. The practical version of the DFT was adapted by Kohn and Sham in 1965 [54], is simply represented in equation 3.4.

$$E[\rho] = T_S[\rho] + J[\rho] + \int \upsilon_s(r)\rho(r)dr + E_{xc} \qquad (3.4)$$

where E denotes the energy, T_s is the kinetic energy of the electrons, E_{xc} is the exchange-correlation energy, υ_s is the external potential and J is the electron-electron repulsive (Coulombic) energy. All of the terms are a function of the electron density function ρ, which is a function of spatial coordinates. All the terms in the sum except E_{xc} are functionals which can be written as a function of electron density . The Kohn Sham equations suggest to approach the kinetic energy of a non-interacting reference system with the same density as the real.

$$T_S = -\frac{1}{2}\sum_{i}^{N}\langle\psi_i|\nabla^2|\psi_i\rangle \tag{3.5}$$

$$\rho(r) = \sum_{i}^{N}|\psi_i(r)|^2 \tag{3.6}$$

where ψ_i refers to the orbitals of the non-interacting system. T_S is not equal to the real kinetic energy of the system, thus, Kohn and Sham introduced seperation of the universal functional which delivers the ground state energy of the system, $F[\rho]$ is represented in equation 3.7.

$$F[\rho] = T_S[\rho] + J[\rho] + E_{xc}[\rho] \tag{3.7}$$

where the so-called exchange-correlation energy, $E_{xc}[\rho]$, is defined in equation 3.8:

$$E_{xc}[\rho] = (\ T[\rho] - T_S[\rho]\ ) + (\ E_{ee}[\rho] - J[\rho]\ ) \tag{3.8}$$

The Kohn-Sham effictive potential, υ_{eff} given in equation 3.9.

$$\upsilon_{eff}(\mathrm{r}) = \upsilon_s(\mathrm{r}) + \int\frac{\rho\acute{r}}{|r-\acute{r}|}d\acute{r} + \upsilon_{xc}(\mathrm{r}) \tag{3.9}$$

The exchange-correlation potential, $\boldsymbol{\upsilon_{xc}}$ is the functional deriative of E_{xc} with respect to the electron density function ρ (Equation 3.10).

$$\upsilon_{xc}(\mathrm{r}) = \frac{\delta E_{xc}[\rho]}{\delta\rho(r)} \tag{3.10}$$

Finally, the correct density can be obtained by solving the N one-electron equations that is given in equation 3.11.

$$\left[-\frac{1}{2}\nabla^2 + \upsilon_{eff}(\mathrm{r})\right]\psi_i = \epsilon_i\psi_i \tag{3.11}$$

3.3 Nudged Elastic Band (NEB)

In condensed matter physics and theoretical chemistry, the description of a lowest energy path which is also called as “minumum energy path” (MEP) for a rearrangement of structures from one stable composition to another is a common and significant problem. At this point, Nudged Elastic Band (NEB) is an efficient method which is able to find saddle points and MEP between defined final and initial points. This method constructs images along the reaction path, and it optimizes these images to find the MEP. The minimization of this reaction path and optimization of the images are performed by adding spring forces along the path between images and by projecting out parallel component of the true force. The force on image, i, is represented in equation 3.12:

$$\overrightarrow{F_i^0} = -\vec{\nabla}V\left(\overrightarrow{R_i}\right) \big| \perp + \overrightarrow{F_i^S} \cdot \hat{\tau}_{\parallel} \; \hat{\tau}_{\parallel} \tag{3.12}$$

where $\overrightarrow{F_i^S}$ is given in equation 3.13.

$$\overrightarrow{F_i^S} \equiv k_{i+1}\left(\overrightarrow{R_{i+1}} - \overrightarrow{R_i}\right) - k_i\left(\overrightarrow{R_i} - \overrightarrow{R_{i-1}}\right) \tag{3.13}$$

$-\vec{\nabla}V\left(\overrightarrow{R_i}\right) \big| \perp$ is defined in equation 3.14.

$$-\vec{\nabla}V\left(\overrightarrow{R_i}\right) \big| \perp = -\vec{\nabla}V\left(\overrightarrow{R_i}\right) - \vec{\nabla}V\left(\overrightarrow{R_i}\right) \cdot \hat{\tau}_{\parallel} \; \hat{\tau}_{\parallel} \tag{3.14}$$

here $\hat{\tau}_{\parallel}$ refers to the unit tangent to the path, k denotes the spring constant and $\vec{\nabla}V$ is the projection of the perpendicular component. In the literature, $\vec{\nabla}V$ together with the parallel component of the spring force is referred to "nudging". When the relaxed composition of the images satisfies as $\vec{\nabla}V\left(\overrightarrow{R_i}\right) \big| \perp = 0$, the images lie on the MEP and converges to the lowest energy.

4. RESULTS AND DISCUSSIONS

4.1 Global Crystal Structure Predictions

In the first step of the present study, several models were used to perform the crystal structure prediction for strontium metal amine compounds containing different amounts of ammonia. Before the crystal structure predictions, available experimental structures of strontium metal ammine complexes were scannned in the literature. Furthermore, all the crystal structures were predicted by using CASPESA. In the next step , the structures found by CASPESA and the available experimental structures were relaxed at DFT level in order to make energy comparison between them.

4.1.1 Crystal structure predictions for $Sr(NH_3)_8Cl_2$

There are several experimental structures of strontium octaammine complex in the literature. Lysgaard et al. [9] analyzed the structure details of $Sr(NH_3)_8Cl_2$ based on X-ray powder diffraction at 293K. They stated that the unitcell of the octammine is; a = 12.2375 Å, b = 7.4755 Å and c = 15.3455 Å in orthorhombic lattice with a symmetry of Pnma (IT: 62) at 293 K. The experimental structure and its relaxed state can be seen in Figure 4.1.

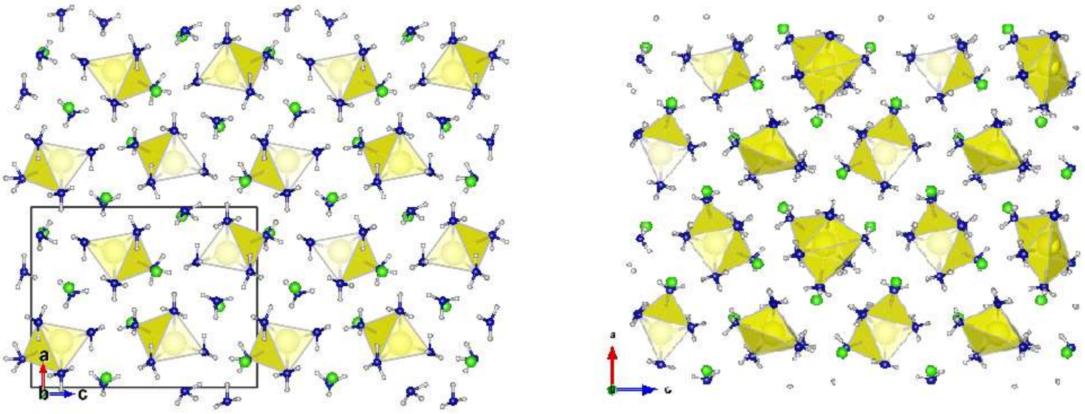

(a) (b)

Figure 4.1 : The experimental and its relaxed structures of $Sr(NH_3)_8Cl_2$. a) The experimental structure at 293K [9]. b) The DFT optimized experimental structure.

In the experimental structure, eight NH_3 molecules bound to Sr atoms with seven bond distances of 2.74 – 2.89 Å and one bond distance of 3.33 Å that form a capped trigonal prism. After the DFT relaxation, the bonds distances between Sr – NH_3 were calculated between 2.72 – 2.93 Å which shows that DFT optimization shrinked the longest bond (Figure 4.2).

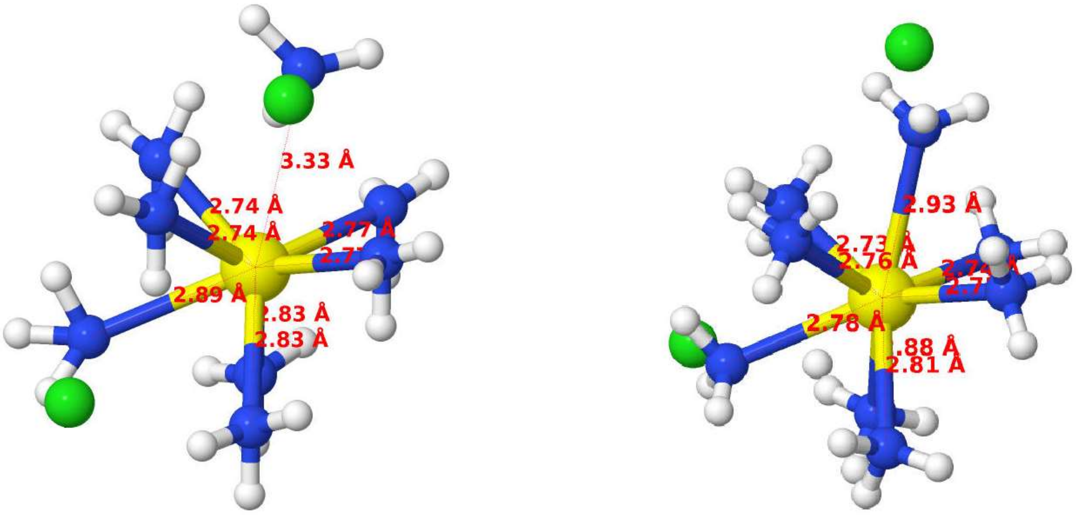

(a) (b)

Figure 4.2 : The bond distances between Sr – N atoms of $Sr(NH_3)_8Cl_2$. a) The experimental structure at 293K [9]. b) The DFT optimized experimental structure.

In another study of strontium octaammine, crystal structures of strontium octaammine were determined at 275 K and 322 K at 2 bar of ammonia pressure [10]. Both of these crystal structures are very similar to the previous experimental structure at 293 K. In all of these structures, Sr atoms with eight NH_3 form a square antiprism in an orthorhombic crystal system with space group of Pnma (IT:62). The interatomic distances between Sr – N are in the range of 2.71 Å to 2.95 Å at 275 K while these distances are between 2.7 Å – 3.6 Å at 322 K at an ammonia pressure of 2 bar. Both structures were relaxed at DFT level and the symmetry of the structure at 275K was not changed, it remained to be Pnma (IT:62). However, the symmetry of the other structure was altered to be Pm (IT:8). The possible reason of this change is the positions of hydrogen atoms. It can be seen in Figure 4.3 that the bond distances of structure at 275 K remained almost same after DFT relaxation. However, some changes were observed in the interatomic distances of the structure at 322 K that the bond distances of the structure were calculated between 2.75 Å to 2.93 Å (Figure 4.4).

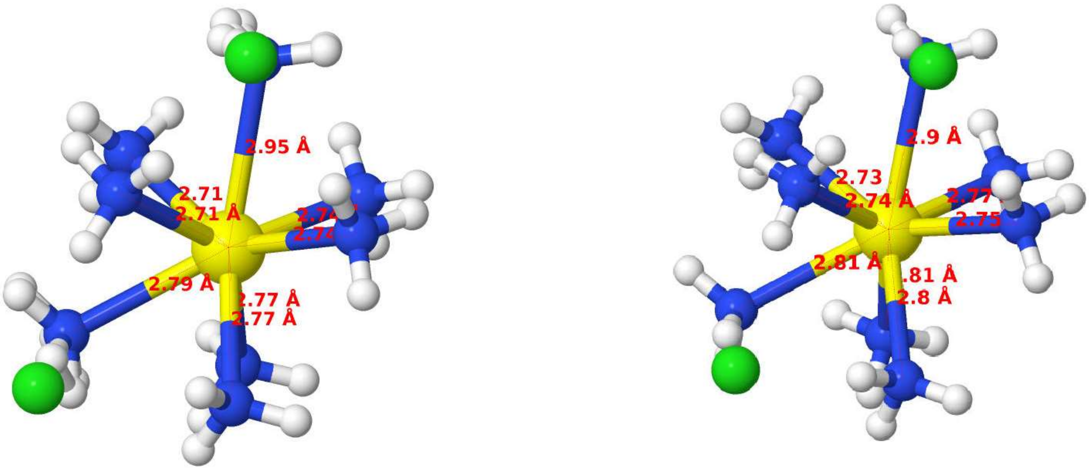
2.95 Å
2.71
2.71 Å
2.79 Å
.77 Å
2.77 Å
2.9 Å
2.73
2.74 Å
2.77
2.75
2.81 Å
.81 Å
2.8 Å

(a) (b)

Figure 4.3 : The bond distances between Sr – N atoms of $Sr(NH_3)_8Cl_2$. a) The experimental structure at 275 K [10]. b) The DFT optimized experimental structure

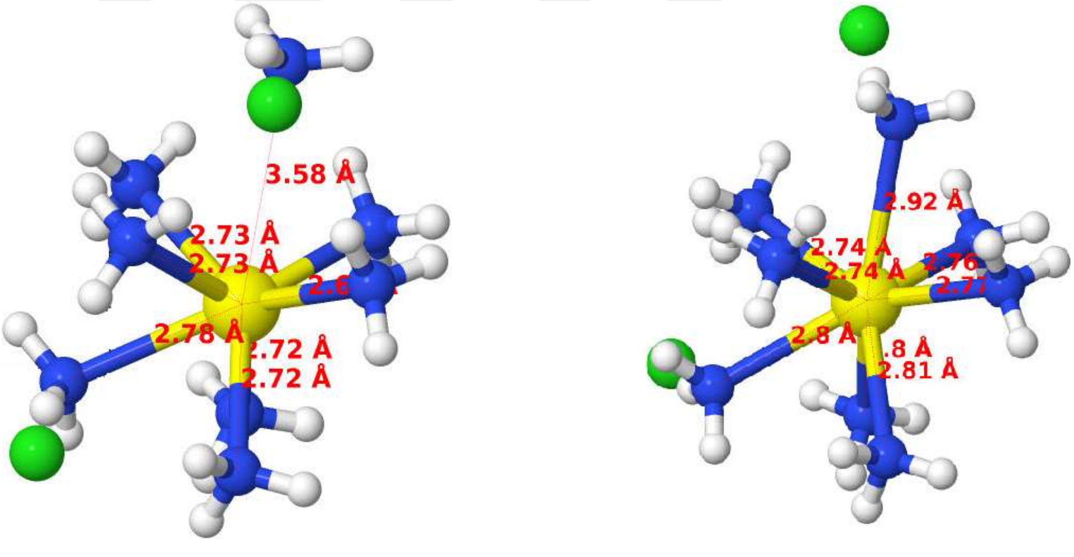
3.58 Å
2.73 Å
2.73 Å
2.78 Å
.72 Å
2.72 Å
2.92 Å
2.74 Å
2.74 Å
2.76
2.77
2.8 Å
.8 Å
2.81 Å

(a) (b)

Figure 4.4 : The bond distances between Sr – N atoms of $Sr(NH_3)_8Cl_2$. a) The experimental structure at 322 K [10]. b) The DFT optimized experimental structure.

After the DFT relaxations of experimental structures, CASPESA were performed for crystal structure predictions of strontium octammine complexes. At this point, six different models were used to predict $Sr(NH_3)_8Cl_2$ complexes as seen in Figure 4.5.

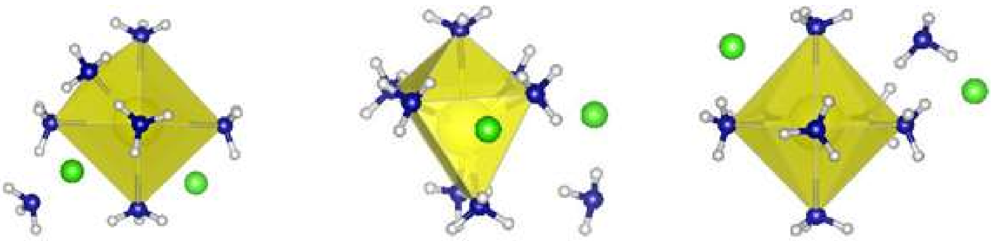

(a) Model 1 (b) Model 2 (c) Model 3

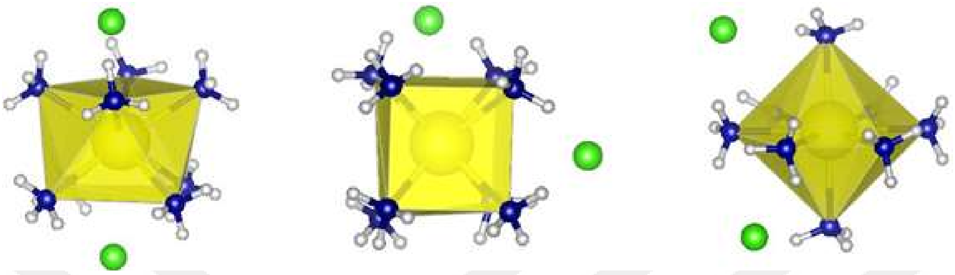

(d) Model 4 (e) Model 5 (f) Model 6

Figure 4.5 : Six different coordination for the structure prediction of $Sr(NH_3)_8Cl_2$.

Model 1, 2 and 3 are constructed with seven NH_3 groups connected to Sr atom and a free NH_3 group allowed to move indepedently while model 4, 5 and 6 are constructed with eight NH_3 groups allowed to move and rotate together with Sr atom. Model 1 is made up of a monocapped octahedron coordination that six NH_3 are placed at equal distance to Sr atom while one NH_3 is located farther than the others. In the second model, seven NH_3 groups with a Sr atom in the center construct capped trigonal prism coordination. In the model 3, two NH_3 groups have axial positions while five of them have equatorial that form a pentagonal bipyramidal molecular geometry. As for model 4, eight NH_3 groups with Sr atom in the center results a anticube shape which is called as square antiprism while they form a cubic coordination in model 5. Model 6 consist of six equatorial and two axial placed NH_3. After the crystal structures of $Sr(NH_3)_8Cl_2$ were predicted by using these models, the selected structures were optimized with DFT calculations. These optimized structures with lowest energies are presented in Figure 4.6. In the structure N8_1 and N8_2, seven NH3 groups form capped trigonal prism arrangement around Sr atom and they contain a free NH_3 in the unitcell. The space group of the structure were found to be Pm (IT:6).

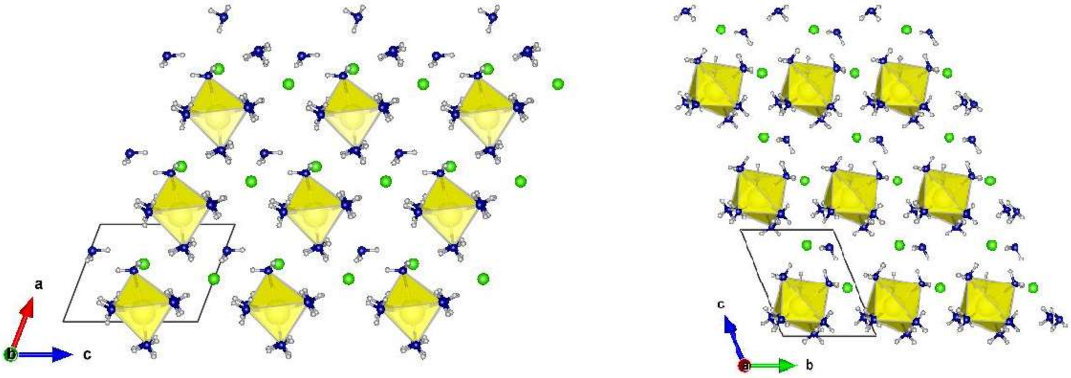

(a) N8_1 (b) N8_2

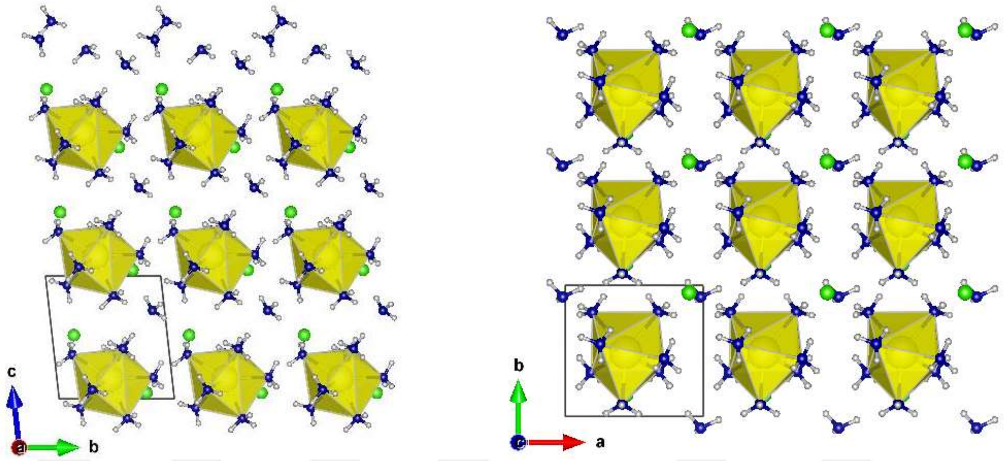

(c) N8_3 (d) N8_4

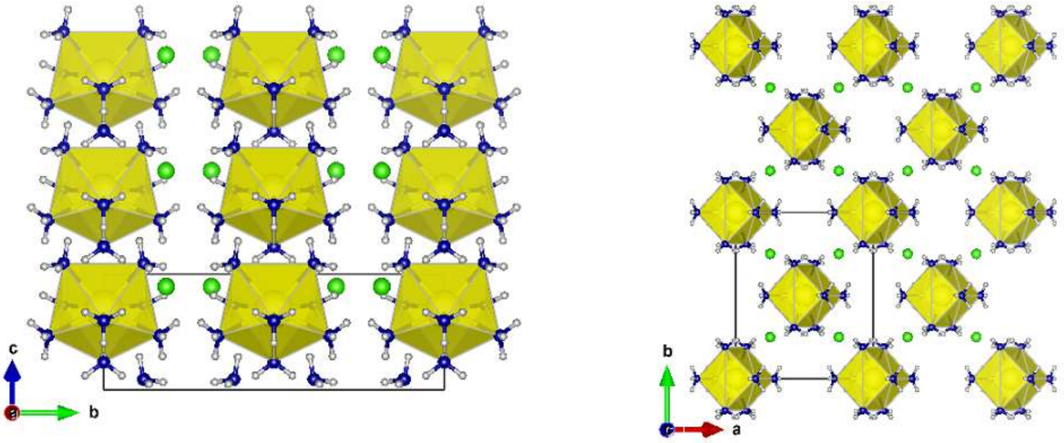

(e) N8_5 (f) N8_6

Figure 4.6 : $Sr(NH_3)_8Cl_2$ structures with the lowest energies

Figure 4.7 illustrates the distances between chlorine and hydrogen atoms in the structure of N8_1 which are between 2.51 Å and 4.23 Å.

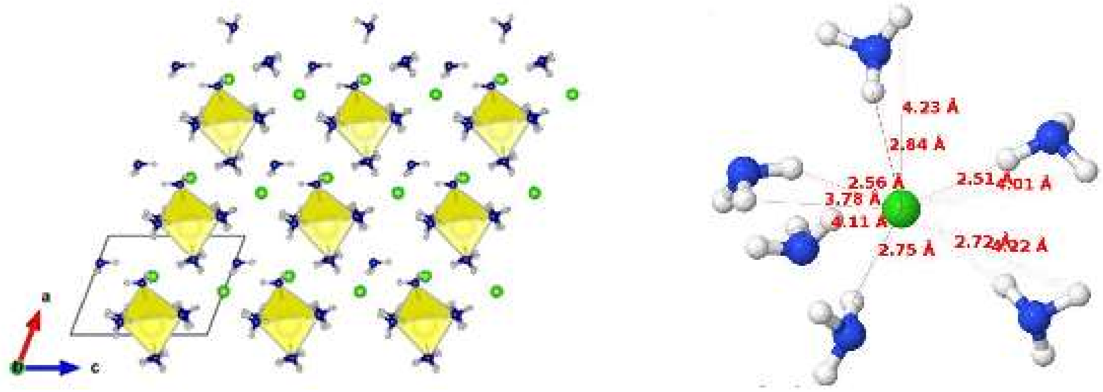

Figure 4.7 : The chlorine – hydrogen distances in N8_1 structure.

The structure N8_3 and N8_4 is also contains a free NH_3 and seven NH_3 groups bounded to Sr atom and they are similar each other as they both have capped octahedron coordination around Sr atom. The only difference is arrangement of free NH_3 and chlorine atoms around $Sr(NH)_3$ group. In the structures N8_5 and N8_6, that is arranged a group around of Sr atoms with eight NH_3. These NH_3 molecules form square antiprism geometry in N8_5 while they form cubic geometry in N8_6. The structure N8_5 have monoclinic crystal system with space group of Cm (IT:8) and N8_6 have space group of C2/m (IT:12).

For all the $Sr(NH_3)_8Cl_2$ structures considered in this study, the energies, crystal symmetries and the cell parameters after the DFT relaxations are given in Table 4.1.

Table 4.1 : The energies, crystal symmetries and the cell parameters of the $Sr(NH_3)_8Cl_2$ structures.

$Sr(NH_3)_8Cl_2$ structures	Energy (eV/f.u)	Space Group	a , b, c (Å)	α, β, γ (°)
N8_1	-4402.3114	Pm (IT:6)	6.91, 7.32, 8.91	90.00, 111.00, 90.00
N8_2	-4402.3105	P1 (IT:1)	6.95, 7.20, 8.97	111.47, 97.12, 91.86
N8_3	-4402. 3053	P1 (IT:1)	7.56, 7.81, 8.24	87.72, 69.55, 67.18
N8_4	-4402.3014	P1 (IT:1)	7.14, 7.21, 8.82	69.59, 85.56, 88.47
275 K [8]	-4402.2810	Pnma (IT: 62)	7.48, 15.34, 12.22	90.00, 90.00, 90.00
N8_5	-4402.2360	Cm (IT:8)	9.69, 15.38, 6.61	90.00, 127.65, 90.00
N8_6	-4402.0198	C2/m (IT:12)	12.01, 12.50, 6.40	90.00, 120.34, 90.00

The new structures predicted by CASPESA were compared with the experimental structure at 257 K which have lower energy than other two experimental structures. It can be seen that the experimental structure and the predicted structures have similar energy values.

4.1.2 Crystal structure predictions for $Sr(NH_3)_6Cl_2$

Two different models were used for the prediction of the $Sr(NH_3)_6Cl_2$, as it can be seen in Figure 4.8.

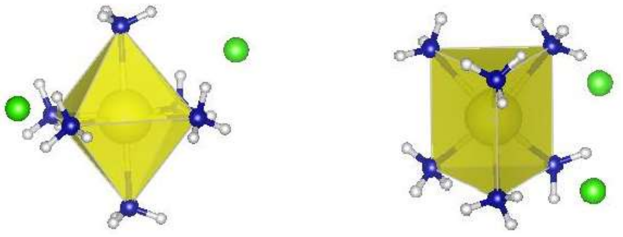

(a) Model 1 (b) Model 2

Figure 4.8 : Two different coordination for the structure prediction of $Sr(NH_3)_6Cl_2$.

Model 1 contains four equatorial and two axial placed NH_3 groups which are connected to Sr atom with octahedral geometry. On the subject of model 2, six NH_3 placed in equal distance to Sr and they construct trigonal prismatic composition. In the next step, the resulting structures were analyzed to select best structures to perform DFT calculations. After the DFT optimization, the lowest energy structures were determined (Figure 4.9). In the N6_1 structure, one of chlorine atoms are placed closer to $Sr(NH_3)$ group and a capped trigonal prism geometry is formed. This structure have hexagonal crystal system with a space group of R3 (IT : 146).

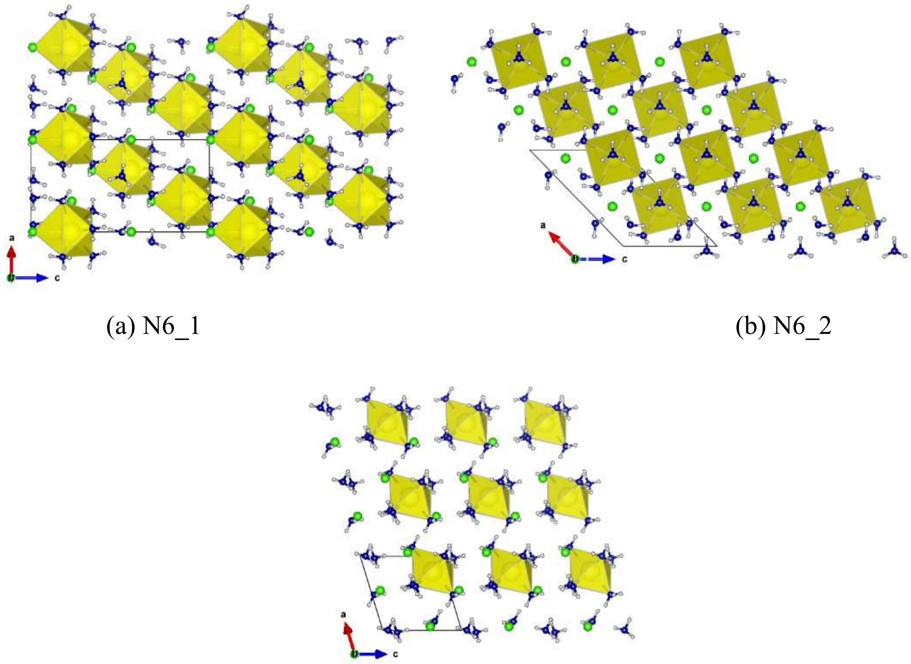

(a) N6_1 (b) N6_2

c) N6_3

Figure 4.9 : $Sr(NH_3)_6Cl_2$ structures with the lowest energies.

Figure 4.10 represents the arrangement of hydrogen atoms around chlorine atoms in the structure of N6_1.

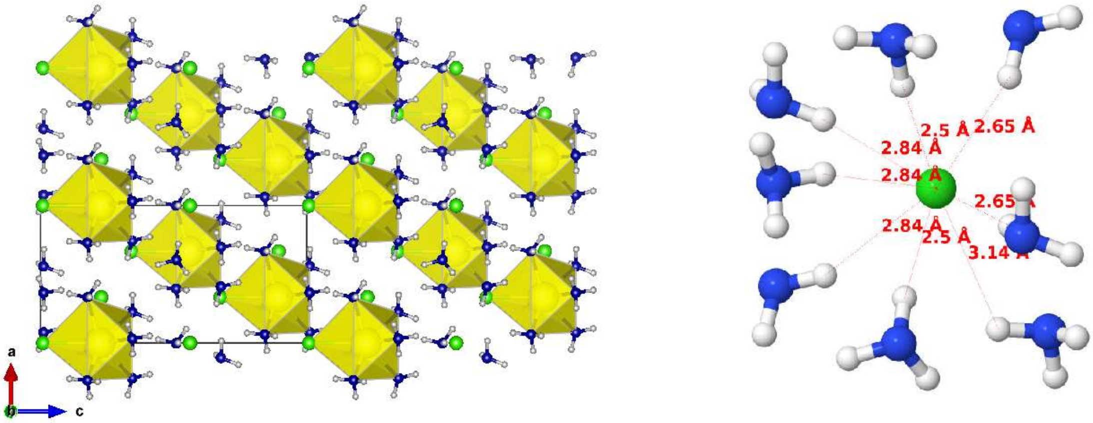

Figure 4.10 : The chlorine – hydrogen distances in N6_1 structure.

In both of N6_2 and N6_3 structures, six NH_3 are in octahedral coordination with Sr atom. They differ in crystal system. The structure N6_2 have monoclinic (Cm) crystal system while N6_3 have triclinic (P-1) crysal system. The cell parameters, crystal symmetries and the energies of these structures are shown in Table 4.2.

Table 4.2 : The energies, crystal symmetries and the cell parameters of the $Sr(NH_3)_6Cl_2$ structures.

$Sr(NH_3)_6Cl_2$ structures	Energy (eV/f.u)	Space Group	a , b, c (Å)	α, β, γ (°)
N6_1	-3761.1981	R3(IT:146)	8.70, 8.70, 14.55	90.00, 90.00, 90.00
N6_2	-3761.0569	Cm (IT:8)	10.71, 11.46, 7.43	90.00, 133.81, 90.00
N6_3	-3761.0563	P-1 (IT:2)	7.46, 7.67, 7.69	118.49, 90.50, 117.36

4.1.3 Crystal structure predictions for $Sr(NH_3)_4Cl_2$

The following two models were used to predict the crystal structure of $Sr(NH_3)_4Cl_2$ (Figure 4.11).

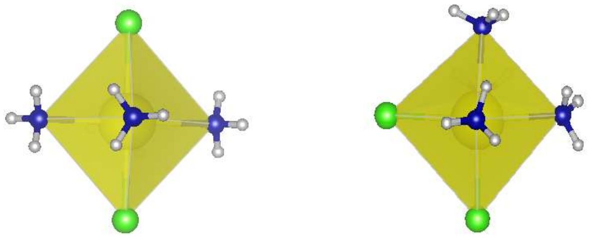

(a) Model 1 (b) Model 2

Figure 4.11 : Two different coordination for the structure prediction of $Sr(NH_3)_4Cl_2$.

In both models, four NH_3 groups and two chlorine atoms are positioned around Sr in octahedral geometry. The first model contains two axial placed chlorine atoms and four equatorial placed NH_3. In the second model, a chlorine atom with a NH_3 group have axial positions and a chlorine atom with three NH_3 groups have equatorial positions. The structures obtained from these models and optimized with DFT is represented in Figure 4.12. All structures have octahedral arrangement. Structure N4_1 and N4_2 have axial located two chlorine atoms and four equatorial located NH_3 while structure N4_3 have two equatorial placed chlorine atom together with two NH_3 and two axial placed chlorine atom with three NH_3 groups. N4_1 and N4_2 is in a monoclinic unitcell with space group C2/m and P2/m respectively and N4_3 is in a triclinic unitcell with space group P-1 (IT:2).

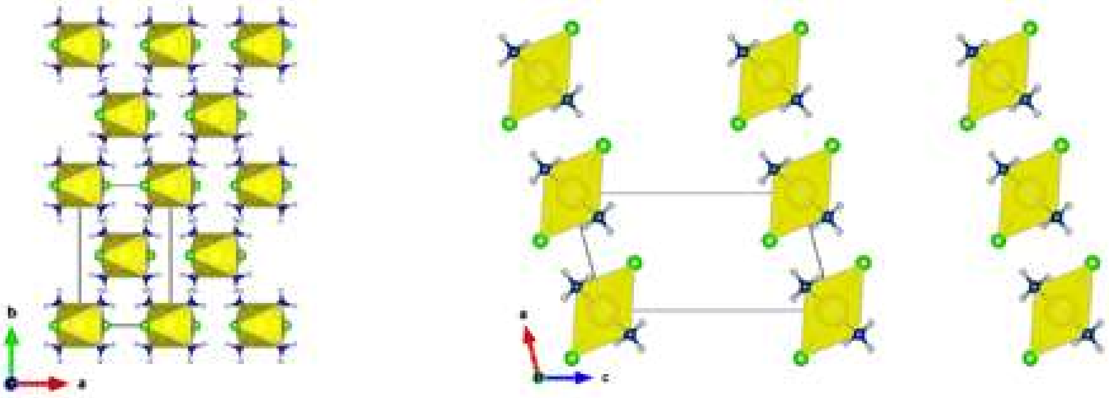

(a) N4_.1 (b) N4_2

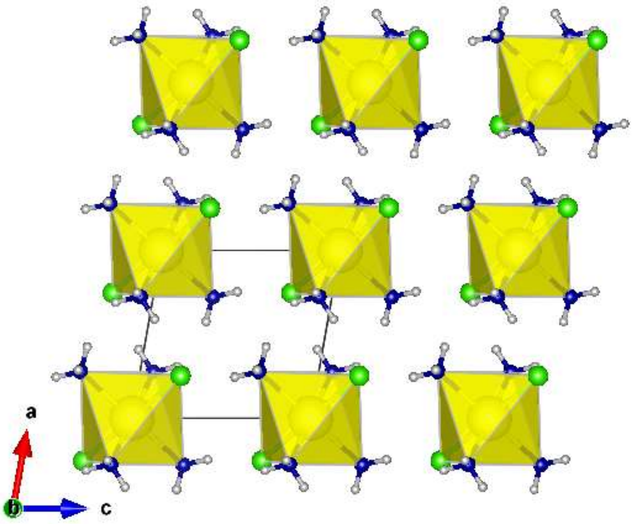

(c) N4_3

Figure 4.12 : $Sr(NH_3)_4Cl_2$ structures with the lowest energies.

The interatomic distances between hydrogen and chlorine atoms in structure N4_1 are illustrated in Figure 4.13.

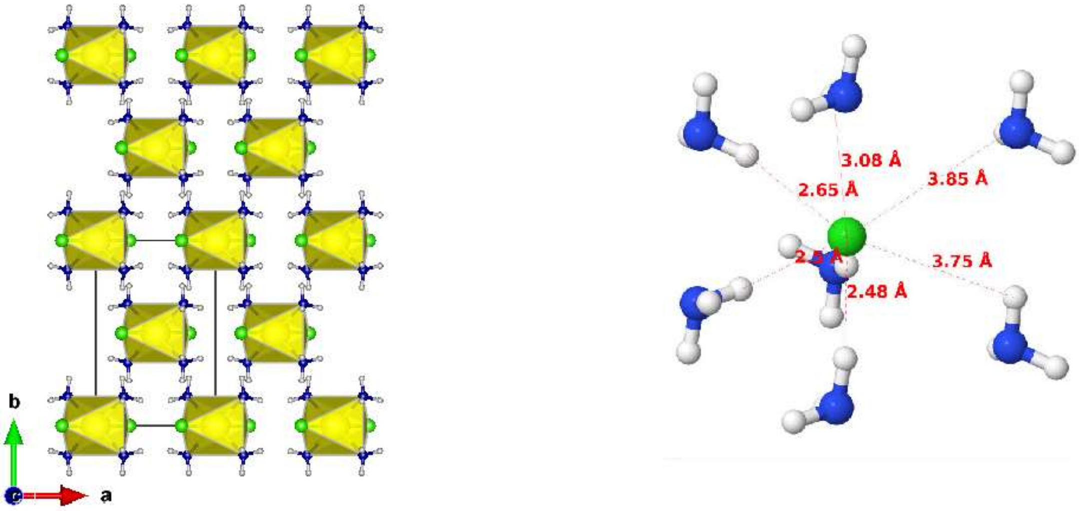

Figure 4.13 : The chlorine – hydrogen distances in N4_1 structure.

In Table 4.3, the cell parameters, crystal symmetries and energies of $Sr(NH_3)_4Cl_2$ structures are represented.

Table 4.3 : The energies, crystal symmetries and the cell parameters of the $Sr(NH_3)_4Cl_2$ structures.

$Sr(NH_3)_4Cl_2$ structures	Energy (eV/f.u)	Space group	a , b, c (Å)	α, β, γ (°)
N4_1	-3119.7953	C2/m(IT:12)	6.96, 10.62, 6.82	90.00, 99.96, 90.00
N4_2	-3119.7331	P2/m(IT:10)	11.750, 8.259, 6.213	90.00, 104.94,90.00
N4_3	-3119.6674	P-1 (IT:2)	6.50, 6.74, 7.26	69.31,78.77,84.58

4.1.4 Crystal structure prediction for $Sr(NH_3)_2Cl_2$

The following model were used in the analysis of $Sr(NH_3)_2Cl_2$ and it can be seen in Figure 4.14. Two axially and equatorially positioned NH_3 molecules aranged in a square planar coordination around Sr atom.

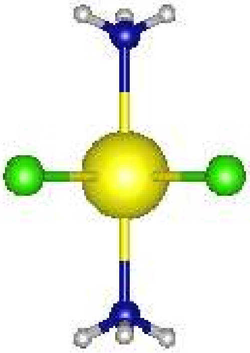

Figure 4.14 : The model used for the crystal structure prediction of $Sr(NH_3)_2Cl_2$.

The structures with the lowest energies obtained from DFT optimization are illustrated in Figure 4.15 and the cell parameters, crystal symmetries and energies of these structures are given in table 4.4. Sr atoms shares two chlorine atoms with the neighbour Sr atom in structure N2_1 where four equatorially located Cl atoms with two axially located NH_3 groups create an octahedral geometry and the structure have monoclinic unitcell with space group C2/m (IT:12). In structure N2_2, Sr atoms share chlorine atoms and create an octahedral coordination. In this octahedral geometry, two NH_3 groups are in the axial positions and four chlorine atoms are in the equatorial positions and the structure prefers a monoclinic unitcell with space group P2/m (IT: 10).

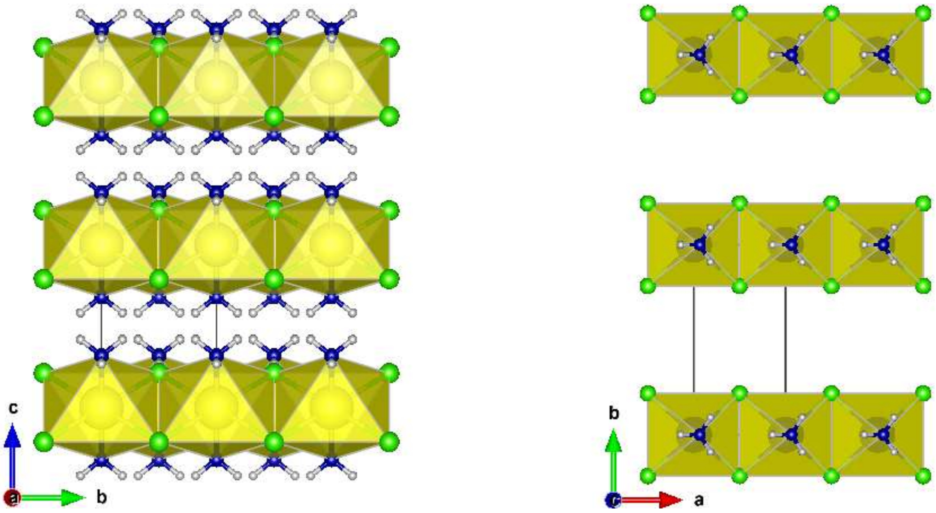

(a) N2_1 (b) N2_2

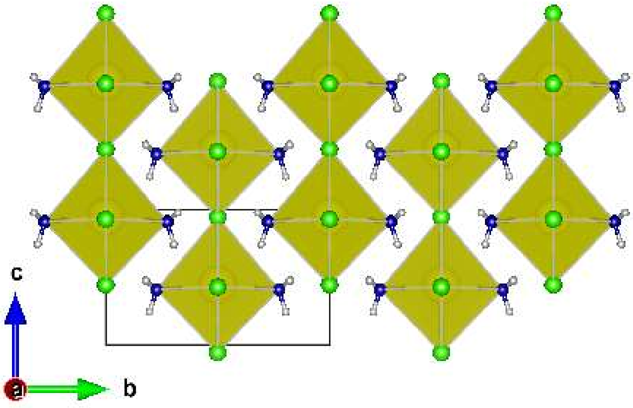

(a) N2_3

Figure 4.15 : $Sr(NH_3)_2Cl_2$ structures with the lowest energies

In the structure N2_3, two NH_3 molecules and two Cl atoms located axially and two Cl atoms located equatorially forms octahedral geometry around Sr atom. This structure prefers a orthorhombic unitcell with space group Imm2 (IT : 44). Figure 4.16

represents the arrangement of hydrogen atoms around chlorine atoms in the structure of N2_1.

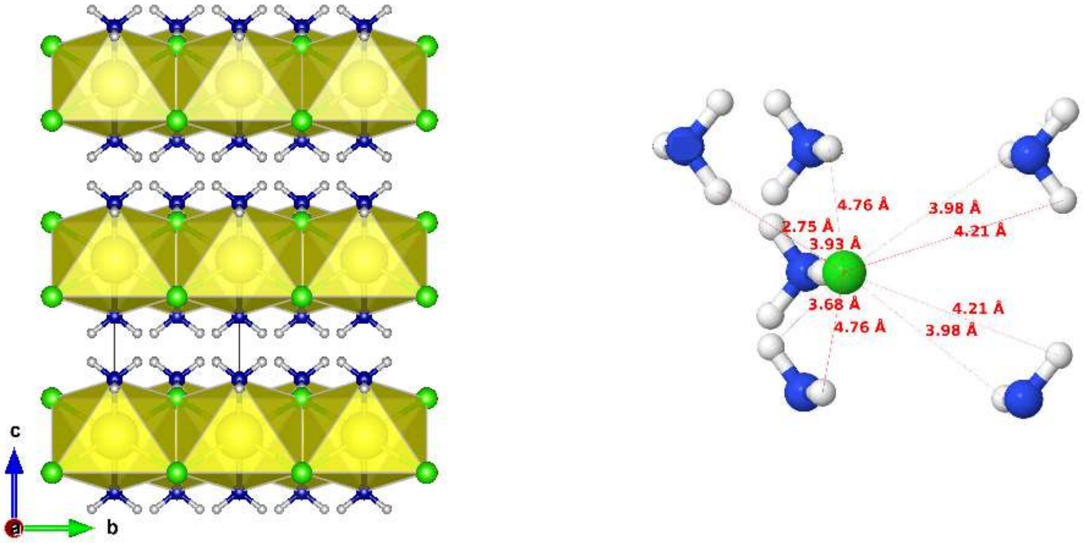

Figure 4.16 : The chlorine – hydrogen distances in N2_1 structure.

The cell parameters, crystal symmetries and the energies of these structures are shown in Table 4.4.

Table 4.4 : The energies, crystal symmetries and the cell parameters of the $Sr(NH_3)_2Cl_2$ structures.

$Sr(NH_3)_2Cl_2$ structures	Energy (eV/f.u)	Space group	a , b, c (Å)	α, β, γ (°)
N2_1	-2478.4995	C2/m (IT:12)	13.51, 4.49, 6.29	90.00, 90.40, 90.00
N2_2	-2478.4885	P2/m (IT:10)	4.38, 9.00, 9.55	90.00, 97.16, 90.00
N2_3	-2478.3327	Imm2(IT:44)	5.91, 9.85, 5.97	90.00, 90.00, 90.00

4.1.5 Crystal structure prediction for $Sr(NH_3)Cl_2$

The following model were used to predict $Sr(NH_3)Cl_2$ crystal structures and the unit cell was modelled using a two formula unit of the structure (Figure 4.17). In the model, two chlorine atoms and NH_3 are in the trigonal planar geometry.

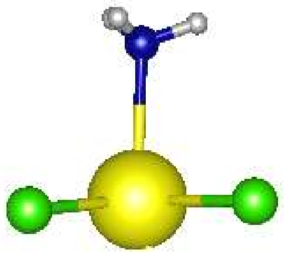

Figure 4.17 : The model used for the crystal structure prediction of $Sr(NH_3)Cl_2$.

The structures of N1_1 have an octahedral geometry with five chlorine atoms and an ammonia molecule. The octahedral arrangement was fused by sharing of three chlorine atoms. In the second structure, capped trigonal prism coordination was arranged by sharing of four chlorine atoms (Figure 4.18). The first structure prefers a monoclinic unitcell with space group of C2/m (IT:12) while the second structure has trigonal unitcell with symmetry of P3m1(IT:156).

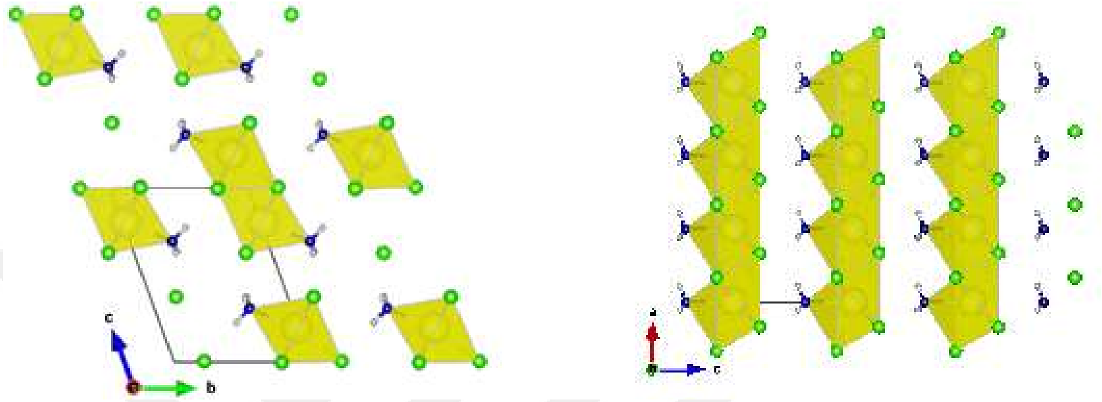

(a) N1_1 (b) N1_2

Figure 4.18 : $Sr(NH_3)Cl_2$ structures with the lowest energies.

The details of the structures are reported in Table 4.5.

Table 4.5 : The energies, crystal symmetries and the cell parameters of the $Sr(NH_3)Cl_2$ structures.

$Sr(NH_3)Cl_2$ structures	Energy (eV/f.u)	Space group	a , b, c (Å)	α, β, γ (°)
N1_1	-2157.6727	C2/m(IT:12)	19.75, 4.43, 7.34	90.00, 110.14, 90.00
N1_2	-2157.6654	P3m1(IT:156)	4.85, 4.85, 6.87	90.00, 90.00, 120.00

4.2 Ammonia Dynamics in Strontium Ammine Complex

After the optimization with DFT, phonon calculations were employed for some of the lowest energy structures especially ones will be used in the Nudged Elastic Band (NEB) calculations.. Phonon dispersion calculations used to examine lattice stability of the structures in order to distinguish the stable structures. In the next step, minumum energy paths (MEP) for NH_3 diffusion and corresponding energy barriers were obtained by NEB method. For the NEB calculations, an ammonia was removed from a supercell to create an ammonia vacancy, then the atomic positions were optimized. Linear interpolation were used between the initial and final states and mostly seven images were used to generate the MEP.

4.2.1 MEP for NH_3 diffusion in $Sr(NH_3)_8Cl_2$

The structures N8_1 and N8_5 were selected to perform NEB calculations. There are many possible transition paths for NH_3 diffusion in $Sr(NH_3)_8Cl_2$ structure. For this structure, both free NH_3 and bulk diffusion of both free and bound NH_3 molecules were considered.. The energy barriers of diffusion were calculated to be 0.47 – 0.6 eV for all the paths. Firstly, the diffusion path of free NH_3 molecule was investigated (Figure 4.19). Nine images were used in between the final and initial states. As clearly seen from the images, free NH_3 (the structure N8_1) moves directly to the final position without any rotation. The corresponding reaction path were found to be 0.47 eV and and no energy difference between the initial and final states was found.

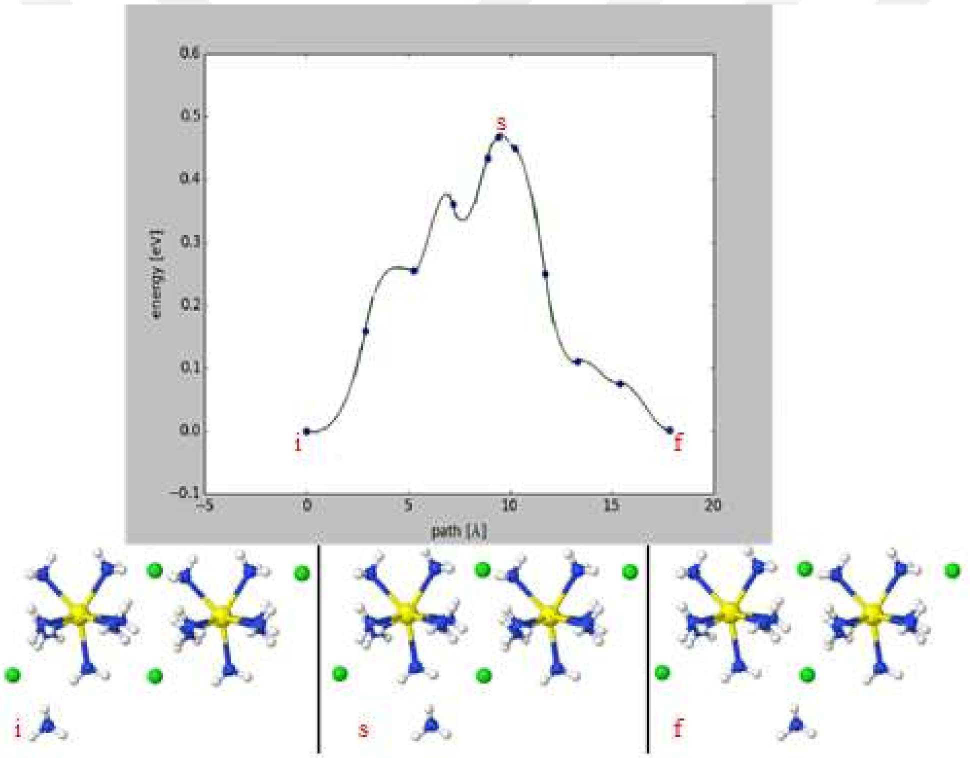

Figure 4.19 : Minumum energy path for free NH_3 diffusion in $Sr(NH_3)_8Cl_2$ (“ i ” refers to initial, “ s ” refers to saddle, and “ f ” refers to final point)

In Figure 4.20, the images show the free NH_3 group rotation around itself and its movement to vacant position on Sr atom. The vacancy formation energy was determined to be 0.51 eV.

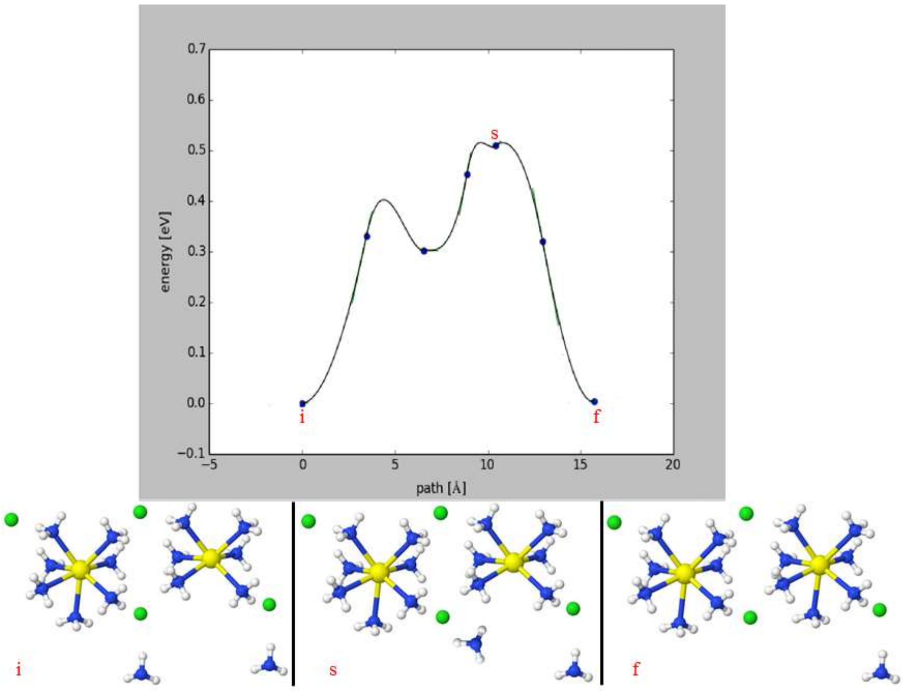

Figure 4.20 : Minumum energy path for free NH_3 diffusion in $Sr(NH_3)_8Cl_2$ (free NH_3 moves to vacant position on Sr atom).

Figure 4.21 illustrates the MEP for bounded NH_3 (for the structure N8_5) molecule moves from Sr to another one. Energy barrier for this arrangement was calculated to be 0.50 eV along the reaction path. In addition, the vacancy formation energy were determined to be 0.54 eV.

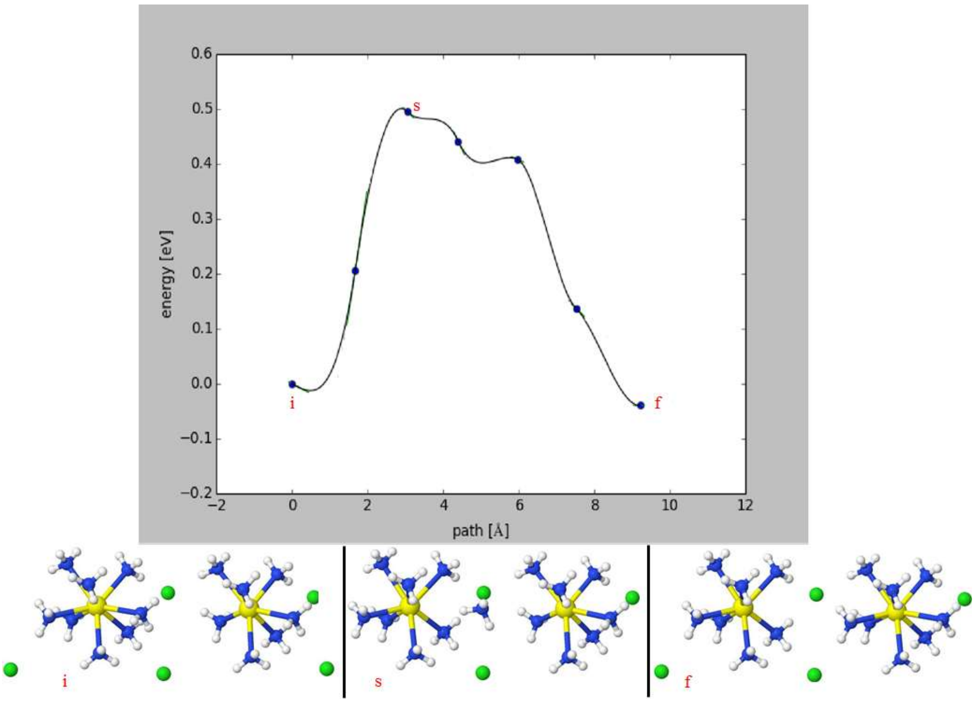

Figure 4.21 : Minumum energy path for bonded NH_3 diffusion in $Sr(NH_3)_8Cl_2$

In the literature [10], it has been stated that the reaction enthalpy for ammonia release from stable octaammine compound at pressure of 1 bar is 41.40 kJ mol^{-1} which is equal to 0.43 eV. It can be seen that literature value of NH_3 desorption enthalpy is close to diffusion barrier calculated by NEB method for strontium octammine structures.

4.2.2 MEP for NH_3 diffusion at $Sr(NH_3)_6Cl_2$

The lowest energy path for diffusion of NH_3 in $Sr(NH_3)_6Cl_2$ complex (the structure N6_1) were determined to be 0.6 - 0.7 eV for various paths. The lowest energy barrier can be seen in Figure 4.22. NH_3 molecule rotate around itself and then goes to vacancy of the next structure and corresponding vacancy formation energy was found to be 0.62 eV and the diffusion energy barrier was calculated to be 0.60 eV. In the study of Tekin et al. [7], vacancy formation energy for magnesium hexammine complex was calculated to be 0.61 eV. They also determined the diffusion energy barrier to be 0.52 eV – 0.60 eV. In comparison, vacancy formation energy values are so close to each other while there is 0.08 eV difference for the lowest diffusion energy barriers.

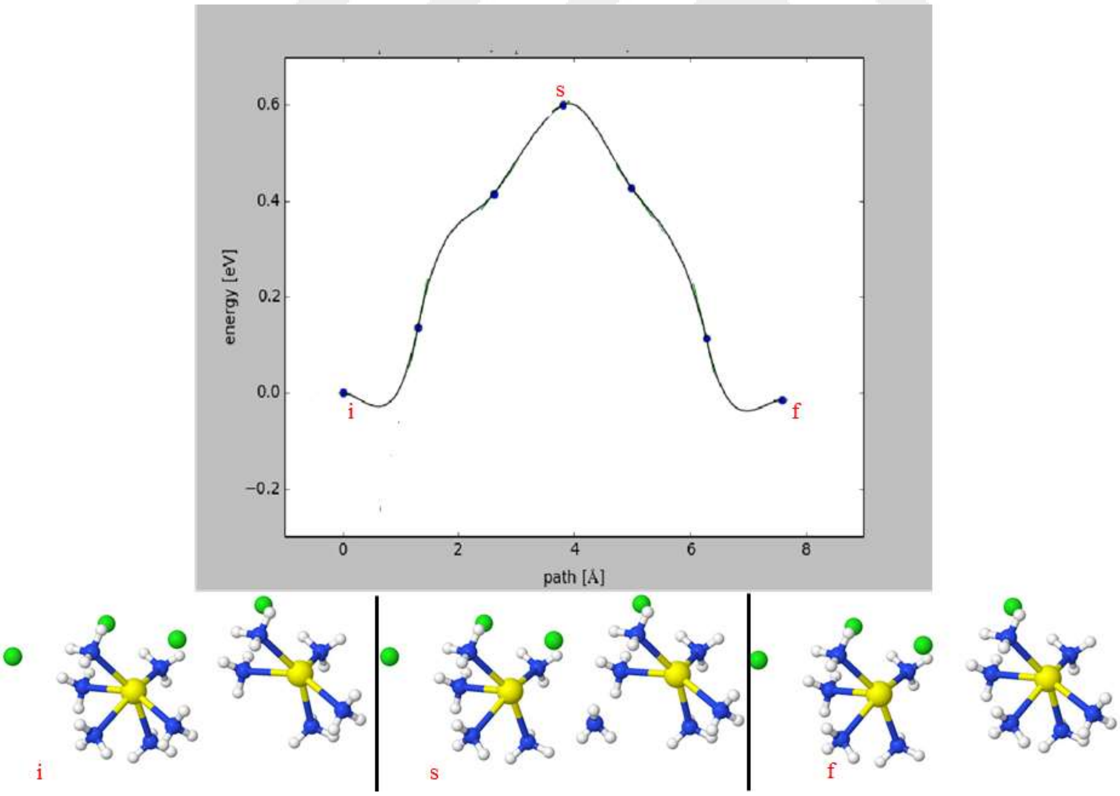

Figure 4.22 : Minumum energy path for NH_3 diffusion in $Sr(NH_3)_6Cl_2$

4.2.3 MEP for NH_3 diffusion in $Sr(NH_3)_2Cl_2$

As seen in images between final and initial states, ammonia molecule moves straightly along the reaction path in strontium diammine structure (the structure N2_1) as seen in Figure 4.23. The energy barrier was calculated to be 0.61 eV and vacancy energy formation was found to be 0.60 eV for this path. In the literature [10], it is stated that desorption enthalpy of NH_3 molecule was determined to be 0.59 eV for diammine.

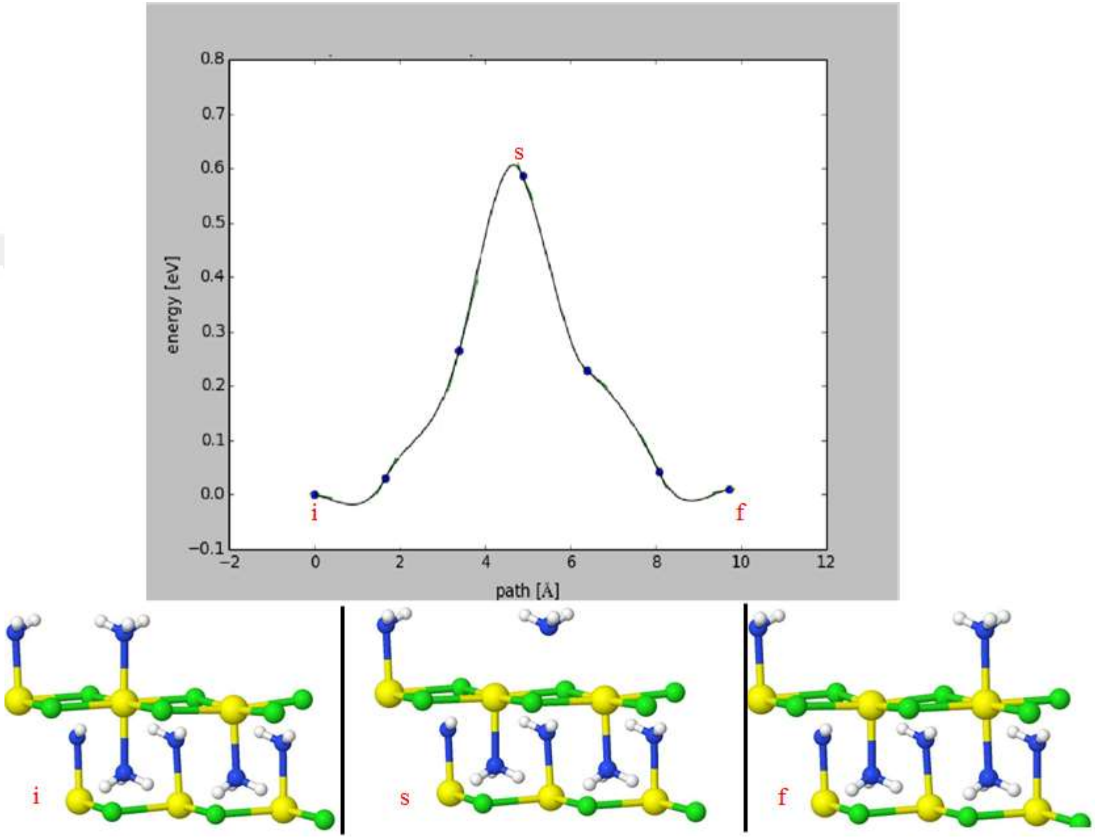

Figure 4.23 : Minumum energy path for NH_3 diffusion in $Sr(NH_3)_6Cl_2$

4.2.4 MEP for NH_3 diffusion in $Sr(NH_3)Cl_2$

The lowest barrier for NH_3 diffusion in monoammine structure (the structure N1_1) was obtained to be 0.65 eV and the vacatn formation energy was found to be 0.63 eV. Single ammonia molecule of the first structure moves to vacant position in the second structure (Figure 4.24). In the literature, enthalpy value for the desorption of ammonia were determined to be 0.50 eV [10].

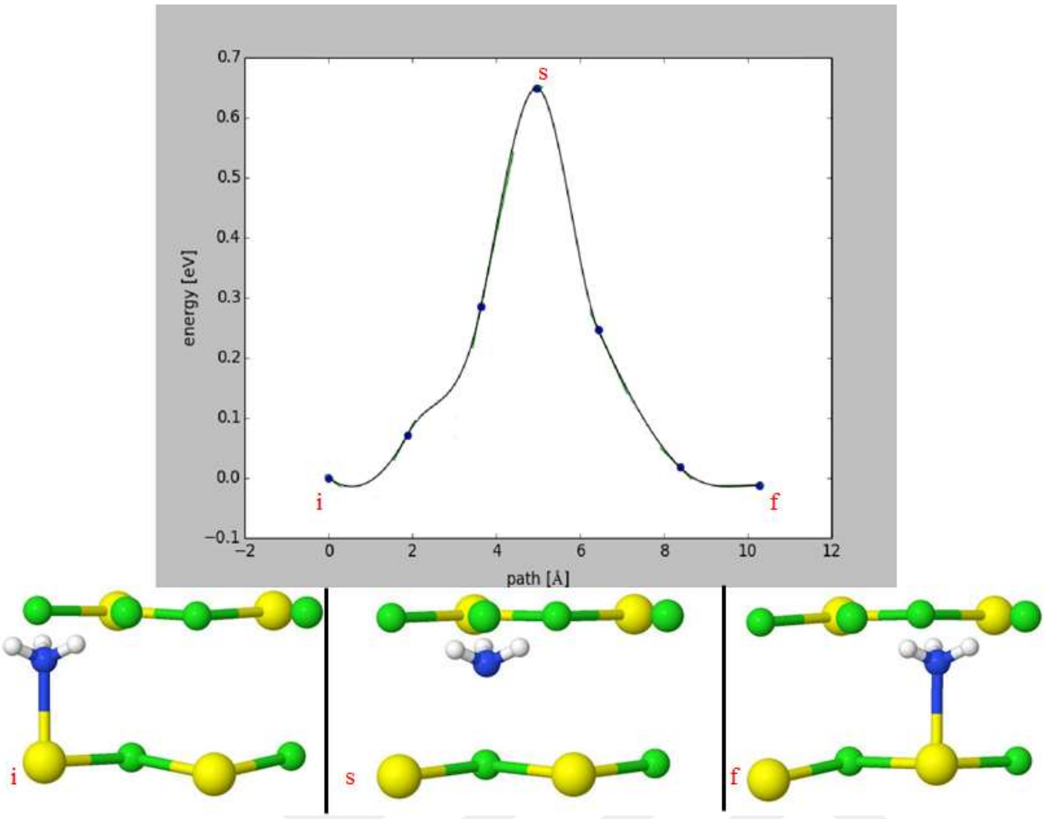

Figure 4.24 : Minumum energy path for NH_3 diffusion in $Sr(NH_3)Cl_2$

The lowest energy barriers and calculated desorption enthalpies were compared with the experimental desorption enthalpies [9] for hexa- to monoammine and monoammine to $SrCl_2$ (Figure 4.25).

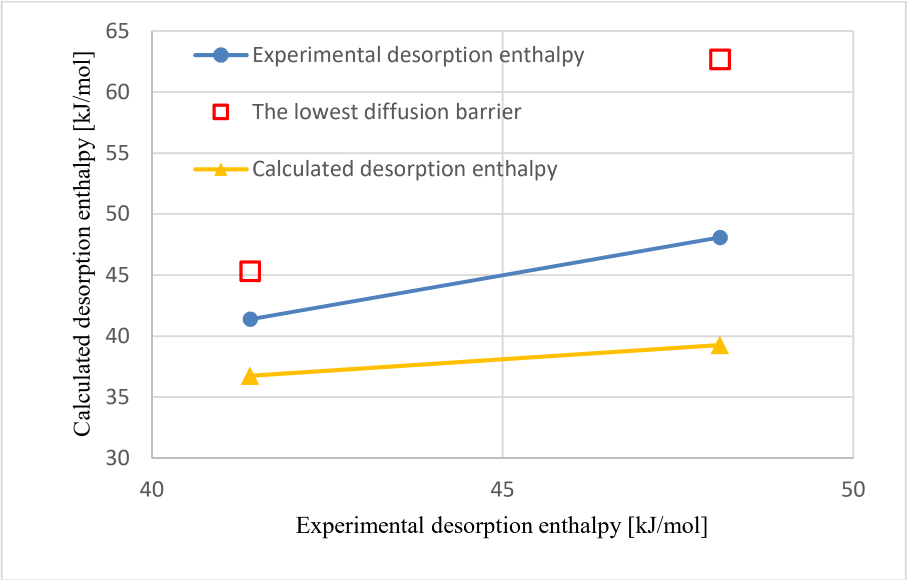

Figure 4.25 : Calculated desorption enthalpies (yellow line) versus experimental desorption enthalpies (blue line) for desorption steps of 8 → 1 and 1 → 0 of strontium ammine. The lowest energy barriers calculated for NH_3 diffusion are represented in red squares.

In Figure 4.26, the lowest energy barriers and calculated desorption enthalpies were compared with the experimental desorption enthalpies [9] for hexa- to di- and di- to monoammine .

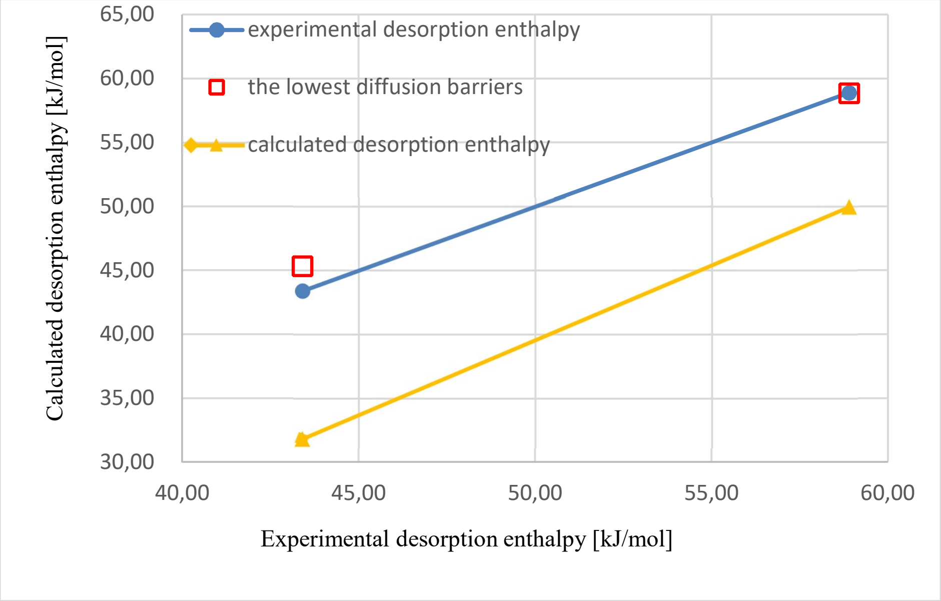

Figure 4.26 : Calculated desorption enthalpies (yellow line) versus experimental desorption enthalpies (blue line) for desorption steps of 8 → 2 and 2 → 1 of strontium ammine. The lowest energy barriers calculated for NH_3 diffusion are represented in red squares.

It is clear that the calculated values were found lower than the experimental desorption enthalpies. However, the calculated values reproduces well the trends observed in the experimental desorption enthalpies and there is a good agreement between the lowest energy barriers and experimental desorption enthalpies.

4.3 Conclusions

The main aim of this study was prediction crystal structures of strontium metal ammine complexes and analysing ammonia dynamics of these structures. For this purpose, firstly the crystal structure prediction program called as CASPESA had been applied succesfully. CASPESA requires some bond constraints and an objective function, thus, experimental structures were scanned in the literature and essential setups were adjusted. The CASPESA was firstly employed for the structure prediction of $Sr(NH_3)_8Cl_2$ which is known experimentally. Several structures were found that have lower in energy than experimental ones. Similarly, CASPESA was used for prediction of the other $Sr(NH_3)_nCl_2$ complexes which contains different number of ammonia molecules (n = 6, 4, 2, 1). Then, these structures were analyzed to select the best structures according to their density, similarity, the coordination type and bond lenghts. The selected structures were further relaxed at the DFT level and several low energy structures with monoclinic, hexagonal and orthorhombic symmetries were obtained. After relaxation at DFT level, phonon dispersion calculations were performed for the lowest energy structures to control their lattice stability. In the next step, minumum energy paths for NH_3 diffusion for the stable structures were calculated by using NEB method. The lowest diffusion energy barriers were found to be 0.47 eV, 0.60 eV, 0,61 eV and 0,65eV for octa-, hexa-, di- and monoammine complexes respectively. In the literature, it is stated that desorption enthalpy of NH_3 molecule was determined to be 0.43 eV and 0.59 eV for hexa- and diammine respectively. It can be seen that there is a good agreement between calculated energy barriers in this study and experimental desorption enthalpies of known structures.

REFERENCES

[1] **Züttel, A.** (2003). Materials for hydrogen storage, *Materials today*, 6(9), 24-33.

[2] **Dinçer, İ.,** (2002). Technical, Environmental and Exergetic Aspects of Hydrogen Energy Systems, *International Journal of Hydrogen Energy*, 27, 265-285.

[3] **Rowsell, J. L. C., Millward, A. R., Park, K. S., and Yaghi, O. M.** (2004). Hydrogen Sorption in Functionalized Metal-Organic Frameworks, *Journal of the American Chemical Society*, 126, 5666-5667.

[4] **Wong-Foy, A. G., Matzger, A. J. and Yaghi., O. M**. (2006). Exceptional H2 Saturation Uptake in Microporous Metal-Organic Frameworks, *Journal of the American Chemical Society*, 128, 3494-3495.

[5] **Christensen, C. H., Sørensen, R. Z., Johannessen, T., Quaade, U. J., Honkala, K., Elmøe, T. D., Køhler, R. and Nørskov, J. K**. (2005). Metal ammine complexes for hydrogen storage, *Journal of Materials Chemistry,* 15, 4106-4108.

[6] **Sørensen, R. Z., Hummelsøhj, J. S., Klerke, A., Reves, J. B., Vegge, T., Nørskov, J. K., and Christensen, C., H.** (2008). Indirect, Reversible High-Density Hydrogen Storage in Compact Metal Ammine Salts, *Journal of the American Chemical Society*, 130, 8660-8668.

[7] **Tekin, A., Hummelshøj, J. S., Jacobsen, H. S., Sveinbjörnsson, D., Blanchard, D., Nørskov, J. K., and Vegge, T.** (2010). Ammonia dynamics in magnesium ammine from DFT and neutron scattering, *Energy & Environmental Science*, 3(4), 448-456.

[8] **Churchard, A. J., Banach, E., Borgschulte, A., Caputo, R., Chen, J. C., Clary, D., Fijalkowski, K. J., Geerlings, H., Genova, R. V., Grochala, W. et al.** (2011). A multifaceted approach to hydrogen storage, *Physical Chemistry Chemical Physics*, 13(38), 16955-16972.

[9] **Lysgaard, S., Ammitzbøll, A. L., Johnsen, R. E., Norby, P., Quaade, U. J., Vegge, T.** (2012). Resolving the stability and structure of strontium chloride amines from equilibrium pressures, XRD and DFT. *International Journal of Hydrogen Energy*, 37, 18927-18936.

[10] **Johnsen, R. E., Jensen, P. B., Norby, P., and Vegge, T.** (2014). Temperature- and Pressure-Induced Changes in the Crystal Structure of Sr(NH3)8Cl2, *The Journal of Physical Chemistry*, 118, 24349-24356.

[11] **Url-1** <*http://www.fysik.dtu.dk/CAMPOS*>, date retrieved 29.09.2015.

[12] **Hammer, B., Hansen, L. B., and Nørskov, J. K.** (1999). Improved adsorption energetics within density-functional theory using revised Perdew-Burke-Ernzerhof functionals, *Phys. Rev. B*, 59, 7413.

[13] **Vanderbilt, D.** (1990). Soft self-consistent pseudopotentials in a generalized eigenvalue formalism, *Phys. Rev. B*, 41, 7892.

[14] **Giannozzi, P., Baroni, S., Bonini, N., Calandra, M., Car, R., Cavazzoni, C., Ceresoli, D., Chiarotti, G. L., Cococcioni, M., Dabo, I. et al.** (2009). QUANTUM ESPRESSO: a modular and open-source software project for quantum simulations of materials. *Journal of Physics: Condensed Matter*, 21(39), 395502.

[15] **Sheppard D., Terrell, R., and Henkelman, G.** (2008). Optimization methods for finding minimum energy paths, *J. Chem. Phys*. 128, 134106.

[16] **Henkelman, G., Jóhannesson, G., and Jónsson, H.** (2000). Methods for Finding Saddle Points and Minimum Energy Paths, *Progress in Theoretical Chemistry and Physics,* 5, 269-302 (2000).

[17] **Henkelman, G., Uberuaga, B. P., and Jónsson, H.** (2000) A climbing image nudged elastic band method for finding saddle points and minimum energy paths, *J. Chem. Phys*., 113, 9901.

[18] **Henkelman, G., and Jónsson, H.** (2000) Improved tangent estimate in the nudged elastic band method for finding minimum energy paths and saddle points, *J. Chem. Phys*., 113, 9978.

[19] **Jónsson, H.,** Mills, G., Jacobsen, K., W. (1998) Nudged Elastic Band Method for Finding Minimum Energy Paths of Transitions, in Classical and Quantum Dynamics in Condensed Phase Simulations, *World Scientific*, 385.

[20] **Wang, Y., Lv, J., Zhu, L., Ma, Y.** (2012). CALYPSO: A method for crystal structure prediction, *Computer Physics Communications*, 183, 2063–2070.

[21] **Kennedy, J., Eberhart, R. C.** (1997). A Discrete Binary Version of the Particle Swarm Algorithm*, IEEE*, 4104 – 4108.

[22] **Eberhart, R.C., Shi, Y.** (2001). Particle Swarm Optimization: Developments, Applications and Resources, *IEEE*, 81-86.

[23] **Hooper, J., Baettig, P., and Zurek, E.** (2012). Pressure induced structural transitions in KH, RbH, and CsH, *Journal of Applied Physics*, 111, 112611.

[24] **Ying, X., Changbo, C., Xiuping, S**. (2014). First-principles study of high-pressure crystal structures and superconductivity of Li3Be alloy, *Computational Materials Science*, 88, 45–49.

[25] **Xiang, H. J., Huang, B., Kan, E., Wei, S. and Gong, X. G.** (2013). Towards Direct-Gap Silicon Phases by the Inverse Band Structure Design Approach, *Physical Review Letters*, 110, 118702.

[26] **Wang, D. Y., Wang, B., and Wang, Y. X.** (2012). New Crystal Structures of IrB and IrB2: First-Principles Calculations, *The Journal of Physical Chemistry*, C116, 21961–21966.

[27] **Jian, L., Yanchao, W., Li, Z., and Ma, Y.** (2011). Predicted Novel High-Pressure Phases of Lithium, *Phys. Rev. Lett*., 106, 015503.

[28] **Glass, C. W., Oganov, A. R., Hansen, N.** (2006). USPEX—Evolutionary crystal structure prediction, *Computer Physics Communications*, 175, 713-720.

[29] **Steele, B. A., and Oleynik, I. I.** (2016). Sodium pentazolate: A nitrogen rich high energy density material*, Chemical Physics Letters*, 643, 21-26.

[30] **Li, Y., and Selloni, A**. (2014). Mosaic Texture and Double c-Axis Periodicity of β-NiOOH: Insights from First-Principles and Genetic Algorithm Calculations, *The Journal of Physical Chemistry Letters*, 5(22), 3981–3985.

[31] **Bilić, A., Gale, J. D., Gibson, M. A., Wilson, N., & McGregor, K.** (2015). Prediction of novel alloy phases of Al with Sc or Ta, *Scientific Reports*, 5, 9909.

[32] **Duan, D., Huang, X., Tian, F., Li, D., Yu, H., Liu, Y., Ma, Y., and Cui, T.** (2015). Pressure-induced decomposition of solid hydrogen sulfide. *Phys. Rev.*, B 91(18), 180502.

[33] **Lonie, D. C, and Zurek, E**. (2011). XtalOpt: An open-source evolutionary algorithm for crystal structure prediction, *Computer Physics Communications,* 182, 372–387.

[34] **Lonie, D. C, and Zurek, E**. (2012). Identifying duplicate crystal structures: XtalComp, an open-source solution, *Computer Physics Communications*, 183, 690–697.

[35] **Falls, Z., Lonie, D. C., Avery, P., Shamp, A., Zurek, E.** (2016). XtalOpt version r9: An open-source evolutionary algorithm for crystal structure prediction, *Computer Physics Communications*, 199, 178-179.

[36] **Url -2** < http://avogadro.openmolecules.net >, date retrieved 27.10.2016.

[37] **Guha, R., Howard, M. T., Hutchison, G. R., Murray-Rust, P., Rzepa, H., Steinbeck, C., Wegner, J., and Willighagen, E. L**. (2006), The Blue ObelisksInteroperability in Chemical Informatics, *J. Chem. Inf. Model*, 46, 991-998.

[38] **Url -3** < http://openbabel.org>, date retrieved 27.10.2016.

[39] **Lonie, D. C., Hooper, J., Altintas, B., and Zurek, E.** (2013). Metallization of magnesium polyhydrides under pressure, *Phys. Rev.*, B87, 054107.

[40] **Hermann, A., Ivanov, B. L., Ashcroft, N. W., and Hoffmann, R.** (2012). LiBeB: A predicted phase with structural and electronic peculiarities, *Phys. Rev*. B86, 014104.

[41] **Url -4** < http://gasp.mse.cornell.edu/>, date retrieved 27.10.2016.

[42] **Tipton, W. W., Bealing, C. R., Mathew, K., Hennig, R. G.** (2013). Structures, phase stabilities, and electrical potentials of Li-Si battery anode materials, *Phys. Rev.*, B87, 184114.

[43] **Tipton, W. K., Hennig, R. G**. (2013). A grand canonical genetic algorithm for the prediction of multi-component phase diagrams and testing of empirical potentials, *J. Phys.: Condens. Matter*, 25, 495401.

[44] **Park, H., Fellinger, M. R., Lenosky, T. J., Tipton, W. W., Trinkle, D. R., Rudin, S. P., Woodward, C., Wilkins, J. W., Hennig, R. G.** (2012). Ab initio based empirical potential used to study the mechanical properties of molybdenum, *Phys. Rev.*, B 85, 214121.

[45] **Bi, W., Meng, Y., Kumar, R. S., Cornelius, A. L., Tipton, W. W., Hennig, R. G., Zhang, Y., Chen, C., Schilling, J. S.** (2011). Pressure-induced structural transitions in europium to 92 GPa, *Phys. Rev.,* B 83, 104106.

[46] **Feng, J., Hennig, R. G., Ashcroft, N. W., Hoffmann, R.** (2008). Emergent reduction of electronic state dimensionality in dense ordered Li-Be alloys, *Nature*, 451, 445–448.

[47] **Bahmann, S., Kortus, J.** (2013). EVO—Evolutionary algorithm for crystal structure prediction, *Computer Physics Communications*, 184, 1618-1625.

[48] **Tekin, A., Caputo, R., and Züttel, A.** (2010). First-principles determination of the ground-state structure of LiBH 4, *Physical review letters*, 104(21), 215501.

[49] **Caputo, R., Tekin, A., Sikora, W., and Züttel, A.** (2010). First-principles determination of the ground-state structure of Mg (BH 4) 2*, Chemical Physics letters*, 480(4), 203-209.

[50] **Caputo, R., Tekin, A**. (2011). Ab-initio crystal structure prediction. A case study: NaBH 4, *Journal of solid state chemistry*, 184(7), 1622-1630.

[51] **Caputo, R., Tekin, A**. (2012). Lithium dihydroborate: first-principles structure prediction of LiBH2, *Inorganic chemistry*, 51(18), 9757-9765.

[52] **Caputo, R., Kupczak, A., Sikora, W., and Tekin, A**. (2013). Ab initio crystal structure prediction by combining symmetry analysis representations and total energy calculations. An insight into the structure of Mg (BH 4) 2, *Physical Chemistry Chemical Physics*, 15(5), 1471-1480.

[53] **Hohenberg, P. and Kohn, W.** (1964). Inhomogeneous electron gas, *Physical review,* 136 (3B), B864.

[54] **Kohn, W. and Sham, L. J**. (1965). Self Consistent Equations Including Exchange and Correlation Effects, *Physical review*, 140, A1133.

CURRICULUM VITAE

Name Surname : Mehmet Çankaya

Place and Date of Birth : İskenderun - 1987

E-Mail : mhmcankaya@gmail.com

B.Sc. : Physics Engineering, Istanbul Technical University